https://dx.doi.org/10.1016/j.engstruct.2017.09.060

Time-Variant Reliability Analysis of Widened Deteriorating Prestressed Concrete Bridges considering Shrinkage and Creep

Bing Tu [a]; Zhi Fang [a,*]; You Dong [b]; and Dan M. Frangopol [c]

[a] College of Civil Engineering, Hunan University, Changsha, Hunan 410082, China

[b] Department of Civil and Environmental Engineering, The Hong Kong Polytechnic University, Hong Kong, China

[c] Department of Civil and Environmental Engineering, Engineering Research Center for Advanced Technology for Large Structural Systems (ATLSS Center), Lehigh University, Bethlehem, PA 18015-4729, USA

Abstract:

Nowadays, bridge widening has become an economic option to tackle the increasing demand of the traffic volume and to enhance the capacity of existing highway bridges. Thus, relevant studies on the performance assessment of widened bridges are needed. This paper presents a computational probabilistic framework for time-variant reliability analysis of widened concrete highway bridges in a systematic manner considering the effects of live-load redistribution, structural deterioration, and concrete shrinkage and creep. Specifically, differences and inconsistences between the new and existing structures regarding live-load distribution, reinforcement corrosion, and concrete shrinkage and creep are considered. A finite element grillage model is constructed to investigate live-load distribution factors and internal axial forces caused by concrete shrinkage and creep. The uncertainties associated with shrinkage and creep effects are accounted for within the probabilistic framework. The flexural moment resistance of the bridge girder is computed considering the combined effects of the shrinkage-and-creep-induced axial force and structural deterioration. Ultimately, the system reliability of the widened bridge is calculated. The proposed probabilistic framework is applied to a widened prestressed concrete T-girder bridge.

Key words: Widened concrete bridge; Live-load distribution factor; Shrinkage and creep; Corrosion; System reliability.

---

*Corresponding author.
E-mail address: fangzhi@hnu.edu.cn (Z. Fang).

1. Introduction

Due to limited budget and conservative prediction of increase of traffic volume, a considerable number of narrow bridges were built previously all over the world. With the rapid growth of traffic volume, many of these existing bridges became functionally obsolete due to insufficient width. Compared with complete replacement or building a new bridge, widening these bridges is generally more economical and effective [1]. For most widened concrete bridges, in order to improve structural integrity, the superstructures of the new and existing bridges are connected by longitudinal splice joints [2]. The static and long-term behavior of the widened bridge, considering the interaction between new and existing bridges, are much more complex than those in the case of treating these bridges separately [3-4]. However, nearly all bridge widening guidelines suggest that standards and guides used for new bridges can also be applied for the widened bridges without considering the interaction between the new and existing bridges [1, 5-8]. Thus, it can be concluded that the specified design and assessment methodology for widened bridges have not been well established and, therefore, relevant studies are needed.

Nowadays, the reliability-based load and resistance factor design (LRFD) method dominates the design philosophy for most current design codes including the Chinese code for design of highway reinforced concrete and prestressed concrete bridge and culverts (JTG D62-2004) [9], the model code 2010 [10], and the AASHTO LRFD Bridge Design Specifications [11], among others. The structural reliability index is also recognized as the fundamental performance indicator for structural safety and performance assessment of existing structures [12-17]. Thus, relevant reliability studies of widened bridges are necessary.

Within the performance assessment of widened bridges, the live-load redistribution should be computed firstly. Nie et al. [18] modified the conventional rigid-jointed girder method (RJGM) to compute the transverse distribution coefficient of concrete girders that are widened with steel-concrete composite beams. Chen et al. [19] proposed a general hinge-jointed slab method (HJSM) for the computation of the lateral distribution factor of widened prestressed concrete hollow slab bridge. Chang et al. [20] investigated the live-load redistribution behavior of widened T-girder and hollow slab bridge using finite element (FE) grillage model. Based on these studies, it can be concluded that the analytical methods (e.g., RJGM, HJSM) are only suitable for certain types of widened bridges, while the FE-model-based method can serve as a general approach for live-load redistribution analysis of widened bridges.

Another well-recognized mechanical characteristic of widened concrete bridges is the shrinkage and creep difference between new and existing girders. This difference could result in significant time-dependent internal stresses [4, 21-23]. Fang et al. [24] investigated the internal forces induced by shrinkage and creep in widened box-girder bridge using FE, and compared the bending moment capacity of the box-girder before and after widening by sectional nonlinear analysis. The results indicated that as the axial compressive force induced by shrinkage and creep changes the failure mode of the existing box-girder (i.e., from flexural failure to compressive-flexural failure), the bending moment capacity of the existing box-girder increases. Thus, it is of vital importance to integrate these effects associated with concrete shrinkage and creep into the structural reliability analysis process. In addition, it should be noted that most studies on shrinkage and creep effects in widened bridges are deterministic. Uncertainties associated with concrete shrinkage and creep will be addressed in this paper.

As bridges are usually directly exposed to environmental attack, their capacities will decrease over time. For reinforced concrete and prestressed concrete bridges, corrosion of reinforcement steel is the primary source of structural deterioration [25-27]. During the past decades, the effects of reinforcement corrosion on the reliability of existing concrete structures have been investigated [28-34]. Two main conclusions can be drawn from these studies. Firstly, reinforcement corrosion plays an important role in time-variant reliability analysis of existing concrete bridges, especially for those exposed to chloride-prone environments [35-37]. Secondly, the deterioration process mainly depends on corrosion initiation time and corrosion rate. As there exist differences in the construction time (or service time) and design profiles (e.g., concrete material properties, thickness of concrete cover) between new and existing girders, the extent of reinforcement corrosion can vary between them. Therefore, it is necessary to consider, for widened concrete bridges, the corrosion progress (i.e., corrosion initiation time and corrosion rate) using time-variant reliability analysis.

Overall, bridge widening has become an economic option to enhance the capacity of existing bridges. However, the reliability analysis of widened bridges is still in its infancy. The interactions between new and existing girders, including live-load redistribution, concrete shrinkage and creep effects, and different reinforcement corrosion, deem to have significant effects on performance of the widened concrete bridges. All these effects should be carefully considered within the reliability assessment process in a systematic and probabilistic manner. Furthermore, the reliability analysis should be conducted at a system level to account for the correlations among different girders and the redundancy of the bridge system. This paper aims to propose a probabilistic approach to compute the time-variant reliability of widened concrete bridges considering live-load redistribution, concrete shrinkage and creep as well as the difference in reinforcement corrosion between new and existing girders. To conduct this study, firstly, live-load distribution factors and internal axial forces caused by concrete shrinkage and creep are computed using a FE grillage model, and an age-adjusted effective modulus (AAEM)-based algorithm is proposed within the FE analysis to assess the shrinkage and creep effects. The uncertainties associated with the shrinkage and creep effects are accounted for within the computation process. Subsequently, considering the combined effects of reinforcement corrosion and the shrinkage-and-creep-induced forces, the probabilistic flexural moment resistance of girder components is assessed using Monte Carlo Simulation (MCS). Then, the superstructure of widened concrete bridge is modeled as a series-parallel system, in which the correlation of resistances between different girder components is considered. Finally, the reliability index of girder components and the bridge system are computed. In order to demonstrate the application of the proposed approach, a widened prestressed concrete T-girder bridge is considered.

2. Flowchart of reliability assessment of widened concrete bridge

The proposed methodology is integrated using three modules: structural analysis of capacity and demand, probabilistic analysis, and system reliability analysis modules, as shown in Fig.1. Firstly, structural analysis of widened concrete bridge is conducted considering the interactions between new and existing girders. The output of this module is the demand (i.e., live-load effect) and resistance of each girder component. Then, the probabilistic analysis module is developed to consider the uncertainties associated with the variables involved in the first module. The simulation methods (e.g., MCS and Latin Hypercube Sampling (LHS) [38]) can be used to generate these random variables. Finally, a system reliability model that describes the behavior of the widened bridge system and the relationship of individual girder components to the overall system is introduced. The reliability of the investigated widened bridge system can be calculated using First order reliability method (FORM)/Second order reliability method (SORM). In order to account for time-dependent effects (i.e., structural deterioration, concrete shrinkage and creep), the proposed methodology is repeated for each time step during the investigated time interval.

3. Live-load redistribution of widened bridge

3.1 Lateral live-load distribution

For a bridge superstructure with multi-girders, the live-load effect on an individual girder is generally computed as [39]

$$F_{refined,i} = F_{beamline} \times g_{F,i} \tag{1}$$

where $F_{refined,i}$ = the maximum live-load flexural moment or shear force in a certain girder for all possible load combinations; $F_{beamline}$ = the maximum flexural moment or shear force determined from a simple beam-line analysis under one lane of traffic; and $g_{F,i}$ = live-load distribution factor (LLDF), which reflects the distribution characteristic of live load in lateral direction.

LLDF is related with many geometric and material parameters, such as girder type, girder spacing, span length, traffic lane arrangement, transverse connection stiffness and sectional longitudinal stiffness, among others [40-42]. As these parameters may change during the bridge widening process, LLDF as well as live-load effect of an individual girder associated with new and existing bridges should be updated accordingly.

Though explicit formulas of LLDF are available in various bridge design codes, such as AASHTO LRFD Specifications [11], these simplified formulas are generally conservative, and are only applicable to certain types of bridges, such as slab-girder superstructures with uniform girder spacing and longitudinal stiffness [43]. For widened bridges, the type of superstructure may vary, and the spacing as well as longitudinal stiffness of girder component of new and existing bridges are usually different. Therefore, a more accurate and systematic method for computation of LLDF of widened structures should be established. Herein, the grillage model is used to compute the LLDF. This method will be described in the following section.

3.2 Grillage model for live-load effect analysis

The grillage-model-based method is adopted herein to compute the live-load effects on bridges before and after widening. Grillage model has been well recognized to produce a good balance between accuracy and computational cost, thus it is usually recommended to analyze complex bridges, such as skewed and curved bridges [44]. The grillage model can be implemented with commercial finite element (FE) software, e.g., *ANSYS* [45], to aid the computational process associated with complex structures. For illustrative purpose, Fig.2(a) shows a typical grillage model of a widened multi-girder bridge. The model consists of eleven longitudinal girders in which girders 1 to 6 are existing girders and 7 to 11 are new girders. Seven transverse members are labeled as a, b, c, d, e, f, g representing the transverse diaphragms. They are uniformly distributed along the span. The rest transverse members are virtual diaphragms, and represent the connection contribution from the girder flange. The splice joint is also modeled as discrete transverse members with corresponding cross section in the grillage model. The precise determination of structural parameters (e.g., flexural stiffness) associated with the splice joint should be based on experimental results and/or a refined FE model. Regarding the engineering applications, some approximations can be made. For instance, in the widened T-girder bridges, flange wet seams and transverse diaphragms are used to connect the adjacent new and existing girders, in which the flexural stiffness of transverse diaphragms is relatively large. Accordingly, the splice joint can be modeled as a rigid connection, as shown in Fig.2(b). For the widened hollow-slab bridge, as the new and old slabs are connected by the weak flange wet seams, it is reasonable to model the splice joint using a hinge connection, as indicated in Fig.2(c). With additional information from test or refined FE modeling regarding splice joint, its model detail can be refined or updated.

4. Concrete shrinkage and creep effects of new and existing bridges

Normally, widening is carried out after several years of service of an existing bridge. By this time, concrete shrinkage and creep in the existing bridge have almost fully developed, while for the newly-built bridge, these long-term deformations just start. Therefore, when subsequent deformations originated from concrete shrinkage and creep of new bridge are restricted by the existing bridge, long-term internal forces (i.e., axial forces and flexural moments) in horizontal plane will generate. The long-term internal forces, especially axial forces, can lead to a significant change of bending capacity of girders [24] and should be carefully considered during the performance assessment process.

4.1 Prediction of concrete shrinkage and creep

The CEB-FIP-90 model [46] has been widely adopted to predict the concrete shrinkage strain and creep coefficient and is used in this study. This model accounts for the effects of several parameters, such as cement type, compressive strength of concrete, theoretical thickness of component, ambient humidity, among others.

Accordingly, the shrinkage strain $\varepsilon_{cs}(t,t_s)$ at time t (days) is calculated as [46]

$$\varepsilon_{cs}(t,t_s)=\left[160+10\beta_{sc}\left(9-f_{cm}/10\right)\right]\beta_{RH}\sqrt{\frac{t-t_s}{350\left(h/100\right)^2+\left(t-t_s\right)}}\times10^{-6} \quad (2)$$

where t_s = concrete age (days) when shrinkage starts; β_{sc} = a coefficient that depends on the type of cement (e.g., for normal or rapid hardening cement, β_{sc} = 5); f_{cm} = mean compressive strength (cylinder) of concrete at the age of 28 days (MPa); h = nominal thickness of member (mm) defined as $2A_c/u$, in which A_c = cross-sectional area and u = perimeter of the member that in contact with the atmosphere; and β_{RH} = a coefficient related to relative humidity of ambient environment, and can be expressed as

$$\beta_{RH} = \begin{cases} -1.55\left[1-\left(RH/100\%\right)^3\right] & 40\% \le RH < 99\% \\ 0.25 & RH \ge 99\% \end{cases} \tag{3}$$

where RH = annual relative humidity of ambient environment (%).

The creep coefficient $\varphi(t,t_0)$ at time t (days) can be calculated as [46]

$$\varphi(t,t_0) = \left[1+\frac{1-RH/100\%}{0.46\left(h/100\right)^{1/3}}\right]\left(\frac{5.3}{\sqrt{f_{cm}/10}}\right)\left(\frac{1}{0.1+t_0^{0.2}}\right)\left[\frac{t-t_0}{\beta_H+\left(t-t_0\right)}\right]^{0.3} \tag{4}$$

where t_0 = initial time when load acting (days), and it corresponds to the widening time; and

$$\beta_H = \min\left\{150\left[1+\left(1.2\frac{RH}{100\%}\right)^{18}\right]\frac{h}{100}+250,\quad 1500\right\} \tag{5}$$

4.2 AAEM-based procedure for analysis of shrinkage and creep

The grillage model, shown in Fig.2(a), is combined with age-adjusted effective modulus (AAEM) method to compute the internal forces caused by the difference of concrete shrinkage and creep between new and existing bridges.

According to AAEM, during the time interval from widening time t_0 to the time of interest t, the relationship between incremental stress $\Delta\sigma(t,t_0) = \sigma(t) - \sigma(t_0)$ and incremental strain $\Delta\varepsilon(t,t_0) = \varepsilon(t) - \varepsilon(t_0)$ of concrete in new bridge can be computed as [47]

$$\Delta\sigma(t,t_0) = E_\varphi(t,t_0)\left[\Delta\varepsilon(t,t_0) - \frac{\sigma(t_0)}{E(t_0)}\varphi(t,t_0) - \varepsilon_{cs}(t,t_0)\right] \tag{6}$$

where $E_\varphi(t,t_0)$ = age-adjusted effective modulus, and can be calculated as [47]

$$E_\varphi(t,t_0) = \frac{E(t_0)}{1+\chi(t,t_0)\varphi(t,t_0)} \tag{7}$$

where $\chi(t,t_0)$ = ageing coefficient that can be derived from $\varphi(t,t_0)$ and $E(t_0)$ = initial elastic modulus.

Eq. (6) can be extended to a generalized vector form as [48]

$$\{\Delta\sigma\} = \left[D_\varphi\right]\left[\{\Delta\varepsilon\} - \left\{\frac{\sigma(t_0)}{E(t_0)}\right\}\varphi(t,t_0) - \{\varepsilon_{cs}\}\right] \tag{8}$$

where $\{\Delta\sigma\}$ = incremental stress vector; $[D_\varphi]$ = effective elasticity matrix, and it can be modified from conventional elasticity matrix by replacing E with $E_\varphi(t,t_0)$; $\{\Delta\varepsilon\}$ = incremental strain vector; $\{\sigma(t_0)/E(t_0)\}$ = initial strain vector caused by initial force $\sigma(t_0)$; and $\{\varepsilon_{cs}\}$ = shrinkage strain vector.

The three strain items in Eq. (8) can be transformed to the corresponding nodal displacement vectors as [48]

$$\{\Delta\varepsilon\} = [B]\{\Delta\delta\}^e \tag{9}$$

$$\begin{Bmatrix} \dfrac{\sigma(t_0)}{E(t_0)} \end{Bmatrix} = [B]\{\delta(t_0)\}^e \tag{10}$$

$$\{\varepsilon_{cs}\} = [B]\{\delta_{cs}\}^e \tag{11}$$

where $[B]$ = strain matrix; $\{\Delta\delta\}^e$ = incremental nodal displacement vector; $\{\delta(t_0)\}^e$ = initial elastic nodal displacement vector caused by initial stress $\sigma(t_0)$; and $\{\delta_{cs}\}^e$ = nodal displacement vector caused by shrinkage.

Then, Eq. (8) can be rewritten as

$$\{\Delta\sigma\} = [D_\varphi][B]\left[\{\Delta\delta\}^e - \{\delta(t_0)\}^e \varphi(t,t_0) - \{\delta_{cs}\}^e\right] \tag{12}$$

Following the principle of conventional finite-element method and neglecting body and surface forces, equilibrium of new bridge element can be established using virtual displacement principle as [48]

$$\int_e [B]^T \{\Delta\sigma\} dV = \{\Delta F\}^e \tag{13}$$

where $\{\Delta F\}^e$ = incremental nodal force vector.

Then, substituting Eq. (12) into Eq. (13), the governing equation for the concrete element of new bridge is derived as

$$[k_\varphi]^e \{\Delta\delta\}^e - [k_\varphi]^e \{\delta(t_0)\}^e \varphi(t,t_0) - [k_\varphi]^e \{\delta_{cs}\}^e = \{\Delta F\}^e \tag{14}$$

$$[k_\varphi]^e = \int_e [B]^T [D_\varphi][B] dV \tag{15}$$

where $[k_\varphi]^e$ = effective stiffness matrix for new bridge elements.

For the existing bridge elements, the effects of concrete shrinkage and creep can be neglected, and the corresponding governing equation is [48]

$$[k]^e\{\Delta\delta\}^e=\{\Delta F\}^e \tag{16}$$

where $[k]^e$ =element stiffness matrix for existing bridge.

Integrating governing equations of all elements (i.e., Eq. (14) and Eq. (16)) into global coordinate system, the governing equation of the entire widened structures is

$$[K]\{\Delta\delta\}-\sum_{new,global}\left[k_\varphi\right]^e\{\delta(t_0)\}^e\varphi(t,t_0)-\sum_{new,global}\left[k_\varphi\right]^e\{\delta_{cs}\}^e=\{\Delta P\} \tag{17}$$

where $[K]$ = global stiffness matrix of the widened structure, in which $[k_\varphi]^e$ and $[k]^e$ are element stiffness matrix used for elements associated with new and existing bridges, respectively; $\{\Delta\delta\}$ = global incremental nodal displacement vector; $\{\Delta P\}$ = global incremental nodal force vector; and $\sum\limits_{new,global}$ means integration of elements within the new bridge under the global coordinate system.

As there is no incremental nodal force during the time interval from the widening time t_0 to the time of interest t, $\{\Delta P\}$ is a zero matrix. Then the Eq. (17) can be transformed as

$$[K]\{\Delta\delta\}=\sum_{new,global}\left[k_\varphi\right]^e\{\delta(t_0)\}^e\varphi(t,t_0)+\sum_{new,global}\left[k_\varphi\right]^e\{\delta_{cs}\}^e \tag{18}$$

Based on the above derivations, the authors developed a computational procedure for FE analysis of shrinkage and creep effects on widened bridge considering the interaction between the new and existing bridges, and the flowchart is shown in Fig.3. The procedure defines the sequence of the analysis process, the pre-processing of input data, and the post-processing of output results. It can be translated into program code and be embedded into arbitrary FE model of widened bridges.

4.3 Analysis of uncertainties

As stated previously, the input (e.g., shrinkage strain and creep coefficient) and the associated calculation model (e.g., FE grillage model and AAEM) in the analysis procedure for shrinkage and creep effects are associated with many parameters, such as concrete material properties (e.g., compressive strength, elastic modulus), geometric parameters (e.g., sectional nominal thickness, area), and environment conditions (e.g., relative humidity), among others. These parameters are usually associated with uncertainty. Thus, it is important to incorporate the uncertainty within the assessment process. Under given information, these parameters can be modeled as random variables with specific distribution types.

Additionally, the modeling uncertainty factors associated with concrete shrinkage strain and creep coefficient prediction (Ψ_1 and Ψ_2) should be incorporated within the computational process. Accordingly, the prediction formula for concrete shrinkage strain $\varepsilon_{cs}(t,t_s)$ and creep coefficient $\varphi(t,t_0)$ (i.e., Eq. (2) and (4)) need to be updated with a multiplicator of Ψ_1 and Ψ_2, respectively. Information on the modeling uncertainty can be obtained from the statistical study conducted by Bažant and Baweja [49]. The mean value and coefficient of variation (COV) of Ψ_1, Ψ_2 within CEB-FIP model are [49]

$$E(\psi_1)=1;\quad V_{\psi_1}=0.451 \tag{19a}$$

$$E(\psi_2)=1;\quad V_{\psi_2}=0.339 \tag{19b}$$

MCS method can be utilized to generate these random variables within the analysis of shrinkage and creep effects. As the finite element simulation (i.e., FE grillage model) process, which aims to establish the implicit relationship between the input (e.g., shrinkage strain and creep coefficient) and output parameters (e.g., internal axial forces), is usually time-consuming, the Latin Hypercube Sampling (LHS) [38] can be used to generate the relevant variables associated with the input and model parameters to improve the computational efficiency.

5. Time-dependent corrosion model

As bridges are usually directly exposed to aggressive environment, their strength and durability degrade with time, and corrosion of reinforcement steel is recognized as the primary source of structural deterioration for reinforced and prestressed concrete bridges [25-27].

Based on the geometric shape of reinforcement steel after corrosion, reinforcement corrosion can be divided into two categories, one is the uniform corrosion that is mainly caused by concrete carbonization and the other is chloride-induced pitting corrosion. According to González et al. [50], the maximum penetration of pitting corrosion is about four to eight times of that associated with uniform corrosion, thus pitting corrosion can lead to a more severe area loss. Therefore, the chloride-induced pitting corrosion is considered in this study. Specifically, area loss and yield (ultimate) strength decrease of reinforcement steel under pitting corrosion are accounted.

The diffusion process of chloride ions through concrete surface is usually modeled by the one-dimensional Fick's law. Accordingly, the corrosion initiation time t_i (years) can be predicted as [25]

$$t_i = \frac{d^2}{4D_c} \frac{1}{\left[erf^{-1}\left(1 - \frac{C_{cr}}{C_0}\right) \right]^2} \tag{20}$$

where d = thickness of concrete cover (cm); D_c = diffusion coefficient of chloride ions (cm^2/year); C_0 = constant concentration of chloride ions on concrete surface (% weight of concrete); C_{cr} = threshold concentration of chloride ions (% weight of concrete); and erf^{1} represents inverse of error function.

Then the radius of the pit in reinforcement bar at time t (years), $p(t)$ (mm), can be computed as [51]

$$p(t) = 0.0116(t - t_i) i_{corr} R \tag{21}$$

where i_{corr} = corrosion current density ($\mu A/cm^2$) and R = the ratio between maximum and average penetration.

The geometric model proposed by Val and Melchers [51] is used to compute the loss of effective cross-sectional area under pitting corrosion. Accordingly, the remain net area of reinforcement bar at time t, $A_r(t)$, is [51]

$$A_r(t)=\begin{cases}\dfrac{\pi D_0^{\,2}}{4}-A_1-A_2, & p(t)\le\dfrac{\sqrt{2}}{2}D_0\\ A_1-A_2, & \dfrac{\sqrt{2}}{2}D_0<p(t)<D_0\\ 0, & p(t)\ge D_0\end{cases} \tag{22}$$

where $a=2p(t)\sqrt{1-\left[\dfrac{p(t)}{D_0}\right]^2}$; $\theta_1=2\arcsin\left(\dfrac{a}{D_0}\right)$; $\theta_2=2\arcsin\left[\dfrac{a}{2p(t)}\right]$; $A_1=\dfrac{1}{2}\left[\theta_1\left(\dfrac{D_0}{2}\right)^2-a\left|\dfrac{D_0}{2}-\dfrac{p^2(t)}{D_0}\right|\right]$; $A_2=\dfrac{1}{2}\left[\theta_2 p^2(t)-a\dfrac{p^2(t)}{D_0}\right]$; and D_0 is the initial diameter of the reinforcement bar.

As the prestressed tendon usually consists of strands with several twisted wires (e.g., seven 5 mm-diameter wires), and is placed inside the grouted corrugated ducts, the corrosion mechanism of prestressed tendons is much more complex than that of reinforcement bar. In this study, the probabilistic model proposed by Darmawan and Stewart [36] is used to account for the corrosion effects of prestressed tendons. This model is based on accelerated corrosion tests of 54 prestressed 7-wire strands and the maximum pit depth $p(t)$ was found to follow an extreme value distribution (type I). Given the corrosion density i_{corr} (μA/cm^2), wire length l (mm) and initial corrosion time t_i (years), the probability distribution function (PDF) of $p(t)$ (cm) is [36]

$$f_{p(t)}(t,i_{corr},l)=\frac{\alpha}{\lambda^{0.54}}\exp\left[-\alpha\left(\frac{p(t)}{\lambda^{0.54}}-\mu\right)\right]\exp\left\{-\exp\left[-\alpha\left(\frac{p(t)}{\lambda^{0.54}}-\mu\right)\right]\right\}\quad t>t_i \tag{23}$$

where

$$\lambda=\frac{D_0^{\,2}-\left[D_0-0.0232i_{corr}(t-t_i)\right]^2}{D_0^{\,2}-\left(D_0-0.0232i_{corr-\exp}T_{0-\exp}\right)^2} \tag{24}$$

$$\mu = \mu_{0-\exp} + \frac{1}{\alpha_{0-\exp}} \ln\left(\frac{l}{l_{0-\exp}}\right), \quad \alpha = \alpha_{0-\exp} \tag{25}$$

Herein, $T_{0\text{-exp}}$ = 0.03836 years, $\mu_{0\text{-exp}}$ = 0.84, $\alpha_{0\text{-exp}}$ = 8.10, $i_{\text{corr-exp}}$ = 186 $\mu A/\text{cm}^2$, $l_{0\text{-exp}}$ = 650 mm and these values are obtained from statistical analysis of the accelerated corrosion tests.

With respect to the prestressed strand with 7 wires, it is assumed that the pitting only formed on the six outer wires [36]. Thus, the remain net area of the entire strand $A_{sr}(t)$ is $6A_{wr}(t) + A_{w0}$, where $A_{wr}(t)$ is the remain net area of outer wire at time t and can be computed using Eq. (22), and A_{w0} denotes the time-invariant net area of the inner wire.

In addition to the loss of net area, existing laboratory results indicate that corrosion could also reduce the yield (ultimate) stress of reinforcement steel by the following equation [52,53]

$$f_y(t) = (1 - 100\alpha_{corr}P_{corr}) f_{y0} \tag{26}$$

where $f_y(t)$ = deteriorated yield (ultimate) stress at time t; f_{y0} = initial yield (ultimate) stress; P_{corr} = percentage of area loss that caused by corrosion (%); and α_{corr} = a coefficient and the value is 0.0054 and 0.0075 for reinforcement bar and prestressed strand, respectively.

6. Illustrative Example

6.1 Bridge description

The presented methodology is applied to a widened simply-supported concrete bridge located in Hebei Province, China. The existing part of the widened bridge was built in 1996, and consisted of 6 prestressed concrete T-shape girders to support three traffic lanes in one direction. In 2016, the existing bridge was widened with another 5 prestressed concrete T-shape girders to expand it to five traffic lanes in one direction, as shown in Fig.4(a). The continuous flange wet seams and seven uniformly-arranged transverse diaphragms are used to connect the girders within the construction and widening process, as shown in Fig.4(b).

The existing and new bridges were designed based on the old and the latest version of Chinese Code for Design of Reinforced Concrete and Prestressed Concrete Highway Bridges and Culverts, i.e., JTJ 023-85 [54] and JTG D62-2004 [9], respectively. The nominal compressive strength f_{ck1} of concrete used in existing bridge is 28.0 MPa [54] and the corresponding nominal compressive strength of the concrete used in the new bridge f_{ck2} is 32.4 MPa [9]. The reinforcement steel (prestressed tendons and reinforcement bars) arrangement in mid-span section of existing and new girders is shown in Fig.4(c) and Fig.4(d), respectively. In Fig.4(c) and Fig.4(d), R_y^b and f_{pk} denote the nominal ultimate stress of prestressed tendon, R_{g1}, R_{g2} and f_{sk} represent the nominal yield stress of reinforcement bar.

Accordingly, the FE grillage model of the illustrated bridge is constructed using *ANSYS* [45], as shown in Fig.5. The longitudinal new and existing girders, the transverse diaphragms, and the transverse virtual diaphragms are modeled using BEAM189 element, a 3-D quadratic finite strain beam. The transverse splice joint members are modeled by rigid connections as shown in Fig.2(b). The cross sections and spatial arrangements of the longitudinal and transverse members are determined according to the bridge configuration as indicated in Fig.4. Linear elastic behavior of all elements is assumed under the effects of live-load and concrete shrinkage and creep. In the analysis for live-load effect, the elastic modulus of concrete of new and existing bridge is 3.45×10^4 MPa [9] and 3.30×10^4 MPa [54], respectively. The analysis for shrinkage and creep effects is conducted according to the incremental procedure indicated in Fig.3. Within the analysis process, the elastic modulus of concrete used in the existing bridge is fixed as 3.30×10^4 MPa. The age-adjusted effective modulus is adopted for concrete in the new bridge, and the value of the age-adjusted effective modulus is updated in each time interval by using Eq. (7).

6.2 Load effects

The flexural failure in the mid-span section, as the dominate failure mode for simply-supported girder, is investigated in this paper. The nominal flexural moment in the mid-span section of a single girder subjected to dead load, $M_{DL,n}$, can be calculated as

$$M_{DL,n} = \frac{\left(W_{DC1} + W_{DC2} + W_{DW}\right) l^2}{8} \tag{27}$$

where W_{DC1} = uniformly-distributed load due to self-weight of the T-type girder, and it depends on the geometry size of girder section and density of concrete material; W_{DC2} = uniformly-distributed load due to traffic barriers; W_{DW} = uniformly-distributed load of wearing surface; and l = span length. The flexural moment associated with the dead load is assumed to fellow a normal distribution, and the mean value and coefficient of variation (COV) are 1.0148 $M_{DL,n}$ and 0.0431, respectively [55].

The nominal live-load flexural moment $M_{LL,n}$ is computed based on the truck load specified in the Chinese General Code for Design of Highway Bridges and Culverts [56]. The axle spacing and weight distribution of the specified semitrailer truck are shown in Fig.6. Then given the grillage model as shown in Fig.5, the largest mid-span live-load flexural moments of each girder for all load cases (in both longitudinal and transverse directions) can be computed with following procedure: (1) the longitudinal position of the truck load is determined using influence line analysis based on the single-girder model, and the worst scenario for the flexural moment in mid-span is the case that the front wheel (30 kN) is placed 1.1 m away from the left support; and (2) in the transverse direction, five load combinations are considered, as shown in Fig.7. In these load combinations, the minimum clearance between two adjacent trucks is 1.3 m, and the minimum clearance between the extreme-exterior wheel and the barrier edge is 0.5 m [56]. The five load combinations are moved from left to right side of the deck at a given fixed step (e.g., 0.1 m for each step), respectively. Then, the load effects of the girders under the loading steps can be computed using the grillage model implemented within *ANSYS*. The computed load effects should be further modified by multiplying lane factor (*m* in Fig.7), and the factor equals to 1.00, 0.78, 0.67, and 0.60 for two, three, four, and five adjacent trucks case, respectively [56]. Ultimately, by searching the corresponding maximum flexural moment of mid-span section under the investigated scenarios (i.e., load combinations and load action positions), the worst scenario in transverse direction under the truck load associated with each girder can be determined.

The probabilistic model proposed in Chinese Standard for Reliability Design of Highway Engineering Structures [55] is utilized to account for the uncertainty associated with vehicle load (i.e., live load) effect. Accordingly, the maximum flexural moment through the lifetime period that caused by vehicle load is assumed to follow an extreme value distribution (type I). For the investigated highway bridge, the design period T is specified as 100 years, then the mean value and COV of the live-load flexural moment are 0.7795 $M_{LL,n}$ and 0.0862, respectively [55].

The uncertainty associated with the dynamic load amplification factor η_{DLA} is also considered. η_{DLA} is affected by many factors, such as road surface roughness, bridge dynamics and vehicle dynamics. The distribution of η_{DLA} used herein is based on the monitoring data of a similar bridge (a simply-supported reinforced concrete bridge with a span of 20m) [55]. Accordingly, η_{DLA} is assumed to follow an extreme value distribution (type I) with a mean value of 1.1776 and COV of 0.0428 [55].

6.3 Time-variant resistance model

The time-variant resistance of the bridge is investigated in this section. According to the stress-block model used in JTG D62 2004, the time-variant flexural moment capacity $M_{u0}(t)$ of the flanged concrete section with both prestressed tendons and normal reinforcement bars (see Fig.8(a) and Fig.8(b)) is given by [9]

$$M_{u0}(t)=\begin{cases} k_{pM}\left[0.85 f_c b_f' x_1(t)\left(h_0-\frac{x_1(t)}{2}\right)+f_s'(t)A_s'(t)\left(h_0-a_s'\right)\right], & x_1(t)\le h_f' \\ k_{pM}\left\{\begin{array}{l} 0.85 f_c\left[b x_2(t)\left(h_0-\frac{x_2(t)}{2}\right)+\left(b_f'-b\right)h_f'\left(h_0-\frac{h_f'}{2}\right)\right] \\ +f_s'(t)A_s'(t)\left(h_0-a_s'\right) \end{array}\right\}, & x_2(t)> h_f' \end{cases} \quad (28)$$

where k_{pM} = modeling uncertainty factor for flexural capacity; f_c = compressive strength of concrete; b'_f = effective width of flange; b = width of web; h_0 = effective height of the section, and it is the distance from the top fiber to the centroid of the tensile steel; h'_f = height of flange; $f_s'(t)$, $A_s'(t)$ = yield strength and area of the compressive reinforcement at time t, and it can be determined based on the corrosion model; a'_s = distance from the top fiber to the centroid of the compressive reinforcement; and $x_1(t)$, $x_2(t)$ = depth of concrete compression block when the concrete compression block is within and exceeds the flange height, respectively.

For the widened bridge, concrete shrinkage and creep effects can lead to time-variant axial compressive force $N_c(t)$ or tensile force $N_t(t)$ in the girder, as seen in Fig.8(c) and Fig.8(d). Considering the axial load effect, the flexural capacity of the girder is [9]

$$M_{uN}(t)=\begin{cases} k_{pMN}\begin{bmatrix} 0.85 f_c b'_f x_{1N}(t)\left(h_0-\dfrac{x_{1N}(t)}{2}-e_s\right)+f'_s(t)A'_s(t)e'_s+ \\ \left(f_s(t)A_s(t)+f_p(t)A_p(t)\right)e_s \end{bmatrix}, & x_{1N}(t)\le h'_f \\ k_{pMN}\left\{\begin{array}{l} 0.85 f_c\left[b x_{2N}(t)\left(h_0-\dfrac{x_{2N}(t)}{2}-e_s\right)+\left(b'_f-b\right)h'_f\left(h_0-\dfrac{h'_f}{2}-e_s\right)\right]+ \\ f'_s(t)A'_s(t)e'_s+\left(f_s(t)A_s(t)+f_p(t)A_p(t)\right)e_s \end{array}\right\}, & x_{2N}(t)>h'_f \end{cases} \tag{29}$$

where $M_{uN}(t)$ = flexural moment capacity of section with axial force; k_{pMN} = modeling uncertainty factor; e_s and e'_s = distance from the section centroid to the centroid of the tensile steel and compressive reinforcement bars, respectively; and $x_{1N}(t)$, $x_{2N}(t)$ = the depth of the equivalent rectangular stress block when the block is within and exceeds the flange height, respectively. $x_{1N}(t)$ and $x_{2N}(t)$ can be obtained based on the equilibrium equation of the calculated section with respect to axial force. For instance, for the case with axial compressive force $N_c(t)$ [9]

$$x_{1N}(t)=\frac{f_s(t)A_s(t)+f_p(t)A_p(t)-f_s'(t)A_s'(t)+N_c(t)}{0.85f_cb_f'} \tag{30}$$

$$x_{2N}(t)=\frac{f_s(t)A_s(t)+f_p(t)A_p(t)-f_s'(t)A_s'(t)+N_c(t)}{0.85f_cb}-\frac{(b_f'-b)h_f'}{b} \tag{31}$$

where $f_p(t)$, $A_p(t)$ = ultimate tensile strength and area of prestressed tendon, respectively.

Given the load effects and capacity, the performance function associated with different girders at time t can be identified as

$$g_i(t)=M_{u,i}(t)-\left(M_{DL,i}+\eta_{DLA}M_{LL,i}\right) \tag{32}$$

where $M_{u,i}(t)$ = flexural resistance (capacity) of mid-span section of girder i at time t; $M_{DL,i}$ = dead load moment; η_{DLA} = dynamic load amplification factor; and $M_{LL,i}$ = live-load moment.

6.4 System reliability of bridge superstructure

In order to compute the reliability at the system level, a model that describes the relationship between the individual components and the relationship of individual girder components to overall system should be identified firstly. A series-parallel model for the investigated widened bridge is shown in Fig.9. In this model, it is assumed that failure of any three adjacent girders will cause the whole structure failure [13].

Once the system failure model is established, the reliability of structural components and system are computed using RELSYS (Reliability of Systems), a FORTRAN 77 computer program [57]. RELSYS firstly computes the reliability of every component in the system using FORM. Then, the system is progressively reduced to a single equivalent component, and equivalent alpha vectors are used to account for the correlations between the failure of different equivalent components. The accuracy of the RELSYS has been ascertained by comparing its results with those computed using Monte Carlo simulation [13, 57-59].

The random variables involved in this study are shown in Table 1, and they can be classified to four categories: (1) geometric parameters and initial material properties; (2) parameters that specified for calculation of concrete shrinkage and creep; (3) corrosion-related parameters; and (4) parameters associated with load effects. The relevant references are also indicated in this table.

6.5 Results and discussion

6.5.1 *Live-load distribution factor*

The comparison of live-load distribution factor (LLDF) of each girder before and after widening is shown in Fig.10. LLDF is determined according to Eq. (1). The maximum flexural moment determined from a simple beam-line analysis, $M_{beamline}$, is 2245 kN·m for the investigated bridge.

It can be observed that the LLDF of all existing girders will decrease after widening. As the existing girders that are close to the splice joint (i.e., girder 5 and 6) turn into the interior girder within the widened bridge, the reduction of LLDF associated with these girders is much more significant than that of other girders. For instance, the LLDF of girder 6 after the widening is around 41% of that before the widening; this value associated with girder 2 is approximately 90% of that before widening.

6.5.2 *Axial force induced by concrete shrinkage and creep*

The axial force induced by concrete shrinkage and creep of the new bridge is presented in Fig.11. The results are obtained from the response of 100 times of FE analysis using grillage model implemented within *ANSYS* (see Fig.5). The relevant random variables within the computational process, such as the variables associated with shrinkage strain and creep coefficient, are generated using the LHS, which could improve the sampling efficiency significantly compared with traditional sampling method.

Results of the Chi-square (χ^2) goodness-of-fit tests indicate that normal distribution is an acceptable approximation for the probability distribution of the axial forces (Fig.11(a)). Given t = 100 years, the expected values of the axial force of all girders are presented in Fig.11(b), and it can be concluded that both tensile and compressive force can result in the girders. For instance, in the existing girders, the girder 1 has tensile force, while the girder 6, which is close to the splice joint, results in compressive force. In contrast, for the new girders, the compressive force is associated with the girders that are far away from the splice joint (e.g., girder 11). In addition, the largest expected values of the compressive and tensile forces among all girders are those associated with girders 6 and 7, respectively. The absolute values of these forces are 3863 kN and 3464 kN, respectively. Therefore, concrete shrinkage and creep has a significant effect on the girders that adjacent to the splice joint, and should not be ignored.

The time-variant mean (μ) and mean plus ($\mu + \sigma$) and minus ($\mu - \sigma$) one standard deviation (σ) of axial force in girder 6 and girder 7 are shown in Fig.11(c) and Fig.11(d), respectively. In accordance with the development law of concrete shrinkage strain and creep coefficient, the mean value as well as standard deviation of axial force increase with time, but with a decreasing rate, and the axial force converges at about 20 years after widening.

In addition, a sensitivity analysis is conducted to sorting the importance of the input variables on the variability of the output parameters (i.e., axial forces of girder) within the analysis for shrinkage and creep effects. The Spearman rank-order correlation coefficient (SRCC), as defined by Eq. (33), is utilized herein. The SRCC has a value that ranges from -1 and 1. A larger absolute value of SRCC indicates a higher contribution of the investigated input variable to the output. Accordingly, the SRCC between the input variable x and output variable y can be computed as [66]

$$r_{x,y} = \frac{\sum_{i=1}^{n}\left(X_i - \overline{X}\right)\left(Y_i - \overline{Y}\right)}{\sqrt{\sum_{i=1}^{n}\left(X_i - \overline{X}\right)^2}\sqrt{\sum_{i=1}^{n}\left(Y_i - \overline{Y}\right)^2}} \tag{33}$$

where n is the sampling size; X_i is the rank of x_i within the sampling set of x, $[x_1, x_2, \ldots, x_n]$; Y_i is the rank of y_i within the result set of y, $[y_1, y_2, \ldots, y_n]$; and $\overline{X}$ and $\overline{Y}$ is the average value of X and Y set, respectively.

Given t = 30 years and 100 years, the SRCCs between the input variables and the output axial force in girder 6 and 7 are presented in Table 2. As indicated, the most important input factor is the modeling uncertainty factor of shrinkage Ψ_1, followed by the nominal thickness of girder h and the modeling uncertainty factor of creep Ψ_2. Thus, the Ψ_1 should be paid special attention within the evaluation process.

6.5.3 *Flexural moment capacity*

At each time step, based on Eqs. (28) - (31), flexural moment capacity of each girder is obtained using MCS with 10,000 samplings. The profiles of the flexural moment capacity of girder 6 and 7 are shown in Fig.12. The Chi-square (χ^2) goodness-of-fit test is utilized to search for the optimum distribution of flexural moment capacity. Using this test, for both cases that whether the effects of the shrinkage-and-creep-induced axial force are considered or not, it is best to describe the statistical distribution of flexural moment capacity using a lognormal distribution. The fitting results are shown in Fig.12(a) and (b). Table 3 lists the statistical parameters of these two cases. As shrinkage and creep can induce compressive and tensile axial force to girder 6 and 7 (see Fig.11(b)), the mean value of flexural moment capacity of these two girders increases and decreases by 27.7% and 21.6%, respectively. This change can be intuitively illustrated by the failure curve of reinforced concrete section under the combined effects of flexural moment M and axial force N [67]. In addition, for both girder 6 and 7, the coefficient of variation (COV) of flexural moment capacity increases significantly after including the effects of the axial force. This is mainly attributed to the variability of the axial force itself (see Fig.11(a)) and the increase of modeling uncertainty for flexural capacity calculation regarding different failure modes. The latter is reflected with the increase of COV for the modeling uncertainty factors used in Eq. (28) and Eq. (29) (i.e., 0.062 for k_{pM} versus 0.1344 for k_{pMN}, as listed in Table 1).

Under the combined effects of the shrinkage-and-creep-induced axial force and corrosion of reinforcement steel, the expected value development of time-variant flexural moment capacity of girder 6 and 7 after widening can be divided into two stages, as shown in Fig.12(c) and Fig.12(d). Within 20 years after widening, the effects of axial force have a larger effect on the structural performance. The expected value of flexural moment capacity of girder 6 and 7 increases and decreases with time, respectively, but both with a decreasing rate. Then, the corrosion of reinforcement steel dominates the structural capacity degradation.

6.5.4 *Time-variant reliability of girder components*

The reliability index of each girder is computed based on the performance function (Eq. (32)) at each time step. The results for girders 3, 6, 7 and 10 are shown in Fig.13. According to GB/T 50283-1999 [55], the reliability index threshold β_T is set as 4.2. From Fig.13(a) and Fig.13(b), it can be concluded that without widening, the reliability index of existing girders begins to decrease after about 25 years' service when corrosion initiations, while the reliability index remains above the threshold value through the design service years (i.e., 100 years).

After widening, the reliability index of existing girders will increase due to the decrease of live-load distribution factor. For instance, at t = 20 years (widening time), the reliability index of girder 3 and 6 is increased by 0.2 and 3.4 after widening, respectively. However, if the effects of the shrinkage-and-creep-induced axial force is included, the reliability index of all girders will drop immediately with a value of 2 - 4 at the widening time under the increased COV of flexural moment capacity. After that, the reliability index mainly depends on the quantity of the shrinkage-and-creep-induced axial force. For girder 6 that has the largest compressive axial force, the reliability index will decrease with time after widening, but with a decreasing rate. The decreasing rate of reliability index in the late stage is lower than that of the case without considering the effects of axial force, as shown in Fig.13(b). In contrast, the reliability index of girder 7 will decrease with time at a relatively high rate, as shown in Fig.13(c). The reliability index of girder 6 and 7 reaches the reliability index threshold at about 15 and 50 years after widening, respectively. For girder 3 and 10, as they are less effected by concrete shrinkage and creep, i.e., the expected value of the shrinkage-and-creep-induced axial force is relatively small (see Fig.11(b)), their reliability index will remain above the threshold value through the service life, as shown in Fig.13(a) and (d).

6.5.5 *Time-variant reliability of superstructure system*

RELSYS is utilized to compute the reliability index of existing and widened bridge systems using a series-parallel model as shown in Fig.9. The correlations among the random variables are assumed herein. Specifically, two extreme scenarios are considered regarding capacity correlation among different girders: (a) independent ($\rho_{Mui,Muj} = 0$); and (b) perfect correlation among different new or existing girders ($\rho_{Mui,Muj} = 1$). The correlation between the new girders and existing girders is assumed to be zero. Given more detailed information (e.g., materials used, construction methods, deterioration scenarios), the correlation effects could be easily updated within the reliability analysis process. Within the computational process for system reliability in RELSYS, the determined correlation coefficients among the random parameters (e.g., capacity of different girders) are used to compute the equivalent alpha vectors, which are then utilized to account for the correlations between the failure of different equivalent components [68]. The results of system reliability are presented in Fig.14.

As shown in Fig.14(a), the system reliability index of existing superstructure without considering correlation is higher than that of any girder, this indicates that the redundancy of bridge system will improve the safety of structure. When the correlation is included, the system reliability index reduces significantly, but is still much higher than reliability index threshold through the service life. When the correlation and effects of shrinkage and creep are considered simultaneously, the system reliability index of the widened bridge reaches the index threshold in about 70 years after widening, as shown in Fig.14(b).

7. Conclusions

This paper presents a computational probabilistic framework for time-variant reliability of individual girders as well as system of widened multi-girders concrete bridges. Additionally, the effects of live-load redistribution, concrete shrinkage and creep and the difference in reinforcement corrosion between new and existing girders are considered within the assessment process. The presented approach is applied to a widened prestressed concrete bridge.

The following conclusions are drawn:

1. The live-load distribution factor (LLDF) of all existing girders is reduced after widening. As the existing external girders that are close to the splice joint turn into interior girders after widening, the reduction of LLDF associated with these girders is

more than 40%.

2. Normal distribution is an acceptable approximation to describe the probability distribution of axial force induced by concrete shrinkage and creep. As the shrinkage-and-creep-induced axial force changes the failure mode of prestressed concrete sections (i.e., from flexural failure to compressive-flexural or tensile-flexural combined failure), the expected value of flexural moment capacity of girder component can increase and decrease when subjected to compressive and tensile axial force, respectively. Simultaneously, due to the considerable variability of the shrinkage-and-creep-induced axial force, as well as the significant increase of modeling uncertainty for flexural capacity calculation regarding different failure modes, the variation of flexural moment capacity of all girders will increase significantly when considering the shrinkage and creep effects.
3. Concrete shrinkage and creep have more significant effects on girder reliability than that of live-load redistribution and reinforcement corrosion, especially for the girders adjacent to splice joint, which are subjected to maximum shrinkage-and-creep-induced axial force. The reliability indices of the existing and new girders adjacent to splice joint reaches the threshold value at about 15 and 50 years after widening, respectively. Therefore, special emphasis, such as carefully assessment and conservative design, should be placed on the girders that adjacent to the splice joint when conducting bridge widening.

4. In addition to the shrinkage and creep effects, capacity correlation among different girders has a considerable impact on the system reliability of widened bridges. When correlation and effects of concrete shrinkage and creep are simultaneously considered, the reliability index of the bridge system reaches the threshold value in about 70 years after widening. Therefore, the correlation among different girders should be carefully estimated.
5. The interaction effects between the new and existing parts within a widened bridge are emphasized in this paper. The thermal variation and prestress loss could also have some effects on the structural performance. Given more information, these effects can also be incorporated within the evaluation process.

Acknowledgements

The support from the National Natural Science Foundation of China (Grant No. 51278182) and the program of China Scholarship Council (File No. 201606130095) are gratefully acknowledged. The first author also wants to express his appreciation for the support from the Engineering Research Center for Advanced Technology for Large Structural Systems (ATLSS Center), Lehigh University, PA, USA, during his visit at Lehigh University in the research group of the last author.

References

[1] ACI Committee 345. Guide for widening highway bridges, ACI 345.2R-13, American Concrete Institute, Michigan, USA; 2013.

[2] Zong Z, Xia Z, Chen Y, Zhao X. State- of- the- art and engineering example analysis of longitudinal connection joints between the new bridges and existing old bridges during bridge widening and constructions. Journal of Fuzhou University (Natural Science Edition) 2009; 37(2):248-60 (in Chinese).

[3] Huang P. Research on Static Behavior of Broaden Spliced Prestressed Concrete T Type Beam Bridges. Journal of Highway and Transportation Research and Development 2010; 27(3):86-92 (in Chinese).

[4] Wen Q. Long-term effect analysis of prestressed concrete box-girder bridge widening. Construction and Building Materials 2011; 25(4):1580-6.

[5] Wipf TJ, Fanous FS, Klaiber FW, Eapen AS. Evaluation of Appropriate Maintenance, Repair and Rehabilitation Methods for Iowa Bridges. Final Report, Iowa DOT Project TR-429; 2003.

[6] SCDOT. SCDOT bridge design manual (Chapter 23: Bridge Widening and Rehabilitation). Columbia (SC): South Carolina Department of Transportation; 2006.

[7] Caltrans. Memo to designers (Chapter 9-3: Bridge Widening existing bridges). Sacramento (CA): California Department of Transportation; 2010.

[8] WIDOT. WisDOT Bridge Manual (Chapter 40: Bridge Rehabilitation). Madison (WI): Wisconsin Department of Transportation; 2016.

[9] JTG D62-2004. Code for design of highway reinforced concrete and prestressed concrete bridge and culverts. Beijing: China Communications Press; 2004

[10] Fédération Internationale du Béton (fib). Model code 2010 -final draft. Fédération Internationale du Béton, Bulletins 65, 66, Lausanne, Switzerland; 2012.

[11] AASHTO LRFD. Bridge design specifications. American Association of State Highway and Transportation Officials; 2014.

[12] Mori Y, Ellingwood BR. Reliability-based service-life assessment of aging concrete structures. Journal of Structural Engineering 1993; 119(5):1600-21.

[13] Estes AC, Frangopol DM. Repair optimization of highway bridges using system reliability approach. Journal of Structural Engineering 1999; 125(7):766-75.

[14] Frangopol DM, Kong JS, Gharaibeh ES. Reliability-based life-cycle management of highway bridges. Journal of Computing in Civil Engineering 2001; 15(1):27-34.

[15] Kong JS, Frangopol DM. Life-cycle reliability-based maintenance cost optimization of deteriorating structures with emphasis on bridges. Journal of Structural Engineering 2003; 129(6):818-28.

[16] Saydam D, Frangopol DM, Dong Y. Assessment of risk using bridge element condition ratings. Journal of Infrastructure Systems 2012; 19(3):252-65.

[17] Barone G, Frangopol DM. Reliability, risk and lifetime distributions as performance indicators for life-cycle maintenance of deteriorating structures. Reliability Engineering and System Safety 2014; 123:21-37.

[18] Nie J, Zhang X, Fan J, Li Y, Xu R. Transverse distribution coefficient of concrete bridges widened with steel-concrete composite beams. Journal of Tsinghua University (Science and Technology Edition) 2010; 50(6):805-9 (in Chinese).

[19] Chen J, Zhao S, Yao J. Method for calculating vehicle load traverse distribution in widening design of existing PPCHS bridge. Engineering Mechanics 2012; 29(9):265-71 (in Chinese).

[20] Chang G, Zhang C, Hu W, Wang P. Influence of Widening and Renovation on Mechanical Performance of Old Bridges. Journal of Chongqing Jiaotong University (Natural Science) 2013; 32(1):836-8 (in Chinese).

[21] Wen Q, Ye J. Analysis of shrinkage and creep effects in widening reinforced concrete girder. Journal of Southeast University (Natural Science Edition) 2006; 36(4):596-600 (in Chinese).

[22] Wen Q, Ye J. Shrinkage and creep new and effects of lateral jointing for old concrete beam. China Journal of Highway and Transport 2007; 20(4):53-7 (in Chinese).

[23] Tu B, Fang Z. Analysis of shrinkage and creep effects on newly-built and existing concrete slab bridge after lateral jointing. China Journal of Highway and Transport 2016; 29(10):66-76 (in Chinese).

[24] Fang Z, Chang H, Yang X, Yuan Y. Transverse effects resulting from concrete shrinkage and creep of widened concrete box girder bridge. China Journal of Highway and Transport 2013; 26(6):65-72 (in Chinese).

[25] Enright MP, Frangopol DM. Probabilistic analysis of resistance degradation of reinforced concrete bridge beams under corrosion. Engineering structures 1998; 20(11):960-71.

[26] Dong Y, Frangopol DM, Saydam D. Time-variant sustainability assessment of seismically vulnerable bridges subjected to multiple hazards. Earthquake Engineering and Structural Dynamics 2013; 42(10):1451-67.

[27] Zhou Y, Gencturk B, Willam K, Attar A. Carbonation-induced and chloride-induced corrosion in reinforced concrete structures. Journal of Materials in Civil Engineering 2014; 27(9):04014245.

[28] Frangopol DM, Lin KY, Estes AC. Reliability of reinforced concrete girders under corrosion attack. Journal of Structural Engineering 1997; 123(3):286-97.

[29] Vu KA, Stewart MG. Structural reliability of concrete bridges including improved chloride-induced corrosion models. Structural safety 2000; 22(4):313-33.

[30] Akgül F, Frangopol DM. Time-dependent interaction between load rating and reliability of deteriorating bridges. Engineering Structures 2004; 26(12):1751-65.

[31] Guo T, Frangopol DM, Han D, Chen Y. Probabilistic assessment of deteriorating prestressed concrete box-girder bridges under increased vehicle loads and aggressive environment. Journal of Performance of Constructed Facilities 2010; 25(6):564-76.

[32] Strauss A, Wendner R, Bergmeister K, Costa C. Numerically and experimentally based reliability assessment of a concrete bridge subjected to chloride-induced deterioration. Journal of Infrastructure Systems 2012; 19(2):166-75.

[33] Pillai RG, Trejo D, Gardoni P, Hueste MBD, Reinschmidt K. Time-Variant Flexural Reliability of Posttensioned, Segmental Concrete Bridges Exposed to Corrosive Environments. Journal of Structural Engineering 2014; 140(8): A4014018.

[34] Frangopol DM, Dong Y, Sabatino S. Bridge life-cycle performance and cost: Analysis, prediction, optimization and decision making. Structure and Infrastructure Engineering 2017; doi: 10.1080/15732479.2016.1267772 (in press).

[35] Val DV, Stewart MG, Melchers RE. Effect of reinforcement corrosion on reliability of highway bridges. Engineering structures 1998; 20(11):1010-9.

[36] Darmawan MS, Stewart MG. Spatial time-dependent reliability analysis of corroding pretensioned prestressed concrete bridge girders. Structural Safety 2007; 29(1):16-31.

[37] Akiyama M, Frangopol DM, Yoshida I. Time-dependent reliability analysis of existing RC structures in a marine environment using hazard associated with airborne chlorides. Engineering Structures 2010; 32(11):3768-79.

[38] McKay MD, Beckman RJ, Conover WJ. Comparison of three methods for selecting values of input variables in the analysis of output from a computer code. Technometrics 1979; 21(2):239-45.

[39] Harris DK. Assessment of flexural lateral load distribution methodologies for stringer bridges. Engineering Structures 2010; 32(11):3443-51.

[40] Barr PJ, Eberhard MO, Stanton JF. Live-load distribution factors in prestressed concrete girder bridges. Journal of Bridge Engineering 2001; 6(5):298-306.

[41] Huo XS, Wasserman EP, Zhu P. Simplified method of lateral distribution of live load moment. Journal of Bridge Engineering 2004; 9(4):382-90.

[42] Hughs E, Idriss R. Live-load distribution factors for prestressed concrete, spread box-girder bridge. Journal of Bridge Engineering 2006; 11(5):573-81.

[43] Yousif Z, Hindi R. AASHTO-LRFD live load distribution for beam-and-slab bridges: Limitations and applicability. Journal of Bridge Engineering 2007; 12(6): 765-73.

[44] Hambly EC. Bridge deck behavior. 2nd ed. E & FN Spon; 1991.

[45] Ansys 17.2 Documentation. Ansys, Inc., Canonsburg, PA, USA; 2017.

[46] CEB-FIP MC 90. Design of concrete structures. CEB-FIP Model Code 1990. Thomas Telford; 1993.

[47] Bažant ZP. Prediction of Concrete Creep Effects Using Age-Adjusted Effective. ACI Journal 1972; 69:212-7.

[48] Zienkiewicz OC, Taylor RL. The finite element method. New York: McGraw-Hill; 1977.

[49] Bažant ZP, Baweja S. Justification and refinements of model B3 for concrete creep and shrinkage 1. Statistics and sensitivity. Materials and structures 1995; 28(7):415-30.

[50] González JA, Andrade C, Alonso C, Feliu S. Comparison of rates of general corrosion and maximum pitting penetration on concrete embedded steel reinforcement. Cement and concrete research 1995; 25(2):257-64.

[51] Val DV, Melchers RE. Reliability of deteriorating RC slab bridges. Journal of Structural Engineering 1997; 123(12):1638-44.

[52] Du YG, Clark LA, Chan AHC. Residual capacity of corroded reinforcing bars. Magazine of Concrete Research 2005; 57(3):135-48.

[53] Vu NA, Castel A, François R. Effect of stress corrosion cracking on stress–strain response of steel wires used in prestressed concrete beams. Corrosion Science 2009; 51(6):1453-9.

[54] JTG D62-85. Code for design of highway reinforced concrete and prestressed concrete bridge and culverts. Beijing: China Communications Press; 1985 (in Chinese).

[55] GB/T 50283-1999. Unified standard for the reliability design of highway engineering structures. Beijing: China Plan Press; 1999 (in Chinese).

[56] JTG D60-2004. General specifications for design of highway bridges and culverts. Beijing: China Communications Press; 2004 (in Chinese).

[57] Estes AC, Frangopol DM. RELSYS: A computer program for structural system reliability. Structural Engineering and Mechanics 1998; 6(8):901-19.

[58] Estes AC, Frangopol DM. Bridge lifetime system reliability under multiple limit states. Journal of Bridge Engineering 2001; 6(6):523-8.

[59] Imai K, Frangopol DM. Reliability-based assessment of suspension bridges: Application to the Innoshima Bridge. Journal of Bridge Engineering 2001; 6(6):398-411.

[60] Attard MM, Stewart MG. A two-parameter stress block for high-strength concrete. ACI Structural Journal 1998; 95(3):305-17.

[61] Mirza SA, Hatzinikolas M, MacGregor JG. Statistical descriptions of strength of concrete. Journal of the Structural Division 1979;105(6):1021-37.

[62] Zhang G, Jin X, Guan Y, Yan X. Sultry weather in Shijiazhuang, China and the influencing factors in 1957-2010. PROGRESSUS INQUISITIONES DE MUTATIONE CLIMATIS 2013; 9(3):199-203 (in Chinese).

[63] Val DV, Trapper PA. Probabilistic evaluation of initiation time of chloride-induced corrosion. Reliability Engineering and System Safety 2008; 93(3):364-72.

[64] Stewart MG, Rosowsky DV. Time-dependent reliability of deteriorating reinforced concrete bridge decks. Structural Safety 1998; 20(1):91-109.

[65] Li Y, Bao W, Guo X, Cheng X. Structural reliability and probabilistic limit state design. Beijing: China Communications Press; 1997 (in Chinese).

[66] Conover WJ, Iman RL. Rank transformations as a bridge between parametric and nonparametric statistics. The American Statistician 1981; 35(3):124-9.

[67] Park R, Paulay T. Reinforced concrete structures. New York: John Wiley & Sons; 1975.

[68] Gollwitzer S, Rackwitz R. Equivalent components in first-order system reliability. Reliability Engineering 1983; 5(2):99-115.

TABLES

Table 1. Description of random variables

Variable	Properties	Mean	COV	Distribution type	Reference
b'_f	Effective width of flange	1.0013*	0.0081	Normal	[55]
b	Width of web	1.032*	0.1019	Normal	[55]
h'_f	Height of flange	1.032*	0.1019	Normal	[55]
h_0	Effective height of section	1.0124*	0.0229	Normal	[55]
a'_s	Distance from the top fiber to the centroid of the compressive reinforcement	1.0178*	0.0496	Normal	[55]
h	Nominal thickness of girder	1.032*	0.1019	Normal	[55]
d	Thickness of concrete cover	1.0178*	0.0496	Normal	[55]
A_s, A'_s, A_p	Initial area of tensile reinforcement, compressive reinforcement and prestressed tendon	1.000*	0.0350	Normal	[55]
$f_{c,e}$ (MPa)	Compressive strength of concrete in existing bridge	34.1	0.16	Normal	[55]
$f_{c,n}$ (MPa)	Compressive strength of concrete in new bridge	39.9	0.15	Lognormal	[60]
$f_{s1,e}$ (MPa)	Initial yield strength of reinforcement bar (grade I) in existing bridge	259	0.1211	Normal	[55]
$f_{s2,e}$ (MPa)	Initial yield strength of reinforcement bar (grade Ⅱ) in existing bridge	369	0.0719	Normal	[55]
$f_{s2,n}$ (MPa)	Initial yield strength of reinforcement bar in new bridge	369	0.0719	Normal	[55], [9]
$f_{p,e}$ (MPa)	Initial ultimate strength of prestressed tendon in existing bridge	1662	0.0142	Normal	[61]
$f_{p,n}$ (MPa)	Ultimate strength of prestressed tendon in new bridge	1932	0.0142	Normal	[61]
RH (%)	Annual relative humidity of ambient environment	54.4	0.075	Normal	[62]
Ψ_1	Modeling uncertainty factor of concrete shrinkage	1.000	0.451	Normal	[49]
Ψ_2	Modeling uncertainty factor of concrete creep	1.000	0.339	Normal	[49]
D_c (cm^2/year)	Diffusion coefficient	0.631	0.2	Lognormal	[63]
C_0 (kg/m^3)	Surface chloride content	15	0.2	Normal	[63]
C_{cr} (kg/m^3)	Threshold chloride concentration	2.0	0.2	Normal	[63]
i_{corr} (μA/cm^2)	Corrosion current density	1.0	0.2	Normal	[50]
R	Penetration ratio	3.00	0.33	Normal	[64]

Variable	Properties	Mean	COV	Distribution type	Reference
$M_{DL,i}$	Dead load moment	1.0148*	0.0431	Normal	[55]
$M_{LL,i}$	Live load moment	0.7995*	0.0862	Extreme value (type Ⅰ)	[55]
η_{DLA}	Dynamic load amplification factor	1.1776	0.0428	Extreme value (type Ⅰ)	[55]
k_{pM}	Modeling uncertainty factor for flexural moment capacity	1.110	0.062	Normal	[65]
k_{pMN}	Modeling uncertainty factor for flexural moment capacity with axial force	1.1389	0.1344	Normal	[65]

* indicates the normalized value divided by nominal value.

Table 2. SRCCs between the input and out variables within the analysis for shrinkage and creep effects

Service time t (years)	Output variable	Input variable				
		$f_{c,n}$ (Compressive strength of concrete in new bridge)	RH (Annual relative humidity of ambient environment)	h (Nominal thickness of girder)	Ψ_1 (Modeling uncertainty factor of shrinkage)	Ψ_2 (Modeling uncertainty factor of creep)
30	Axial force in girder 6	0.078	0.092	0.280	-0.923	-0.196
	Axial force in girder 7	0.003	-0.085	-0.276	0.967	0.060
100	Axial force in girder 6	0.053	0.101	0.207	-0.947	-0.103
	Axial force in girder 7	0.013	-0.074	0.199	0.977	-0.035

Table 3. Statistical parameters of flexural moment capacity at t = 100 years

Girder number	Without axial force effects			With axial force effects		
	Mean (kN·m)	Standard deviation (kN·m)	COV	Mean (kN·m)	Standard deviation (kN·m)	COV
6#	6014	544	0.090	7682	2126	0.277
7#	7686	662	0.086	6025	1230	0.204

FIGURES

Fig.1. Flowchart of reliability assessment of widened concrete bridges

Fig.2. Schematic diagram of grillage model for a widened multi-girders bridge (a) basic grillage model; (b) model of splice joint for widened T-girder bridges; and (c) model of splice joint for widened hollow-slab bridges

Fig.3. Flowchart of the proposed AAEM-based procedure

Fig.4. Bridge configuration (a) mid-span section after widening; (b) bottom view (two new girders and one existing girder are included only); (c) arrangement of reinforcement steel of existing girder (mid-span section); and (d) arrangement of reinforcement steel of new girder (mid-span section) (Units: cm)

Fig.5. FE grillage model of the investigated bridge implemented with *ANSYS*

Fig.6. Axle spacing and weight distribution of the semitrailer truck specified in JTG D60 2004 (a) lateral view; and (b) plan view (Units: m) [56]

Fig.7. Transverse truck load cases and positions (Units: m)

Fig.8. Simplified stress-block model for flexural capacity calculation (a) case without axial force; (b) geometric parameters of simplified section; (c) case with compressive force; and (d) case with tensile force [9]

Fig.9. System reliability model of bridge superstructure

Fig.10. Comparison of live-load distribution factor before and after widening

Fig.11. Axial force of mid-span section caused by concrete shrinkage and creep (a) probability density function associated with girder 7 at t = 100 years; (b) expect value in different girder

at t = 100 years; (c) time-variant value of statistic parameters of girder 6; and (d) time-variant value of statistic parameters of girder 7

Fig.12. Flexural moment capacity profiles (a) probability density function associated with girder 6 at t = 100 years; (b) probability density function associated with girder 7 at t = 100 years; (c) time-variant development of expected value of girder 6; and (d) time- variant development of expected value of girder 7

Fig.13. Time- variant reliability index of single girder (a) girder 3; (b) girder 6; (c) girder 7; and (d) girder 10

Fig.14. Time- variant reliability index of superstructure system (a) existing bridge; and (b) widened whole bridge

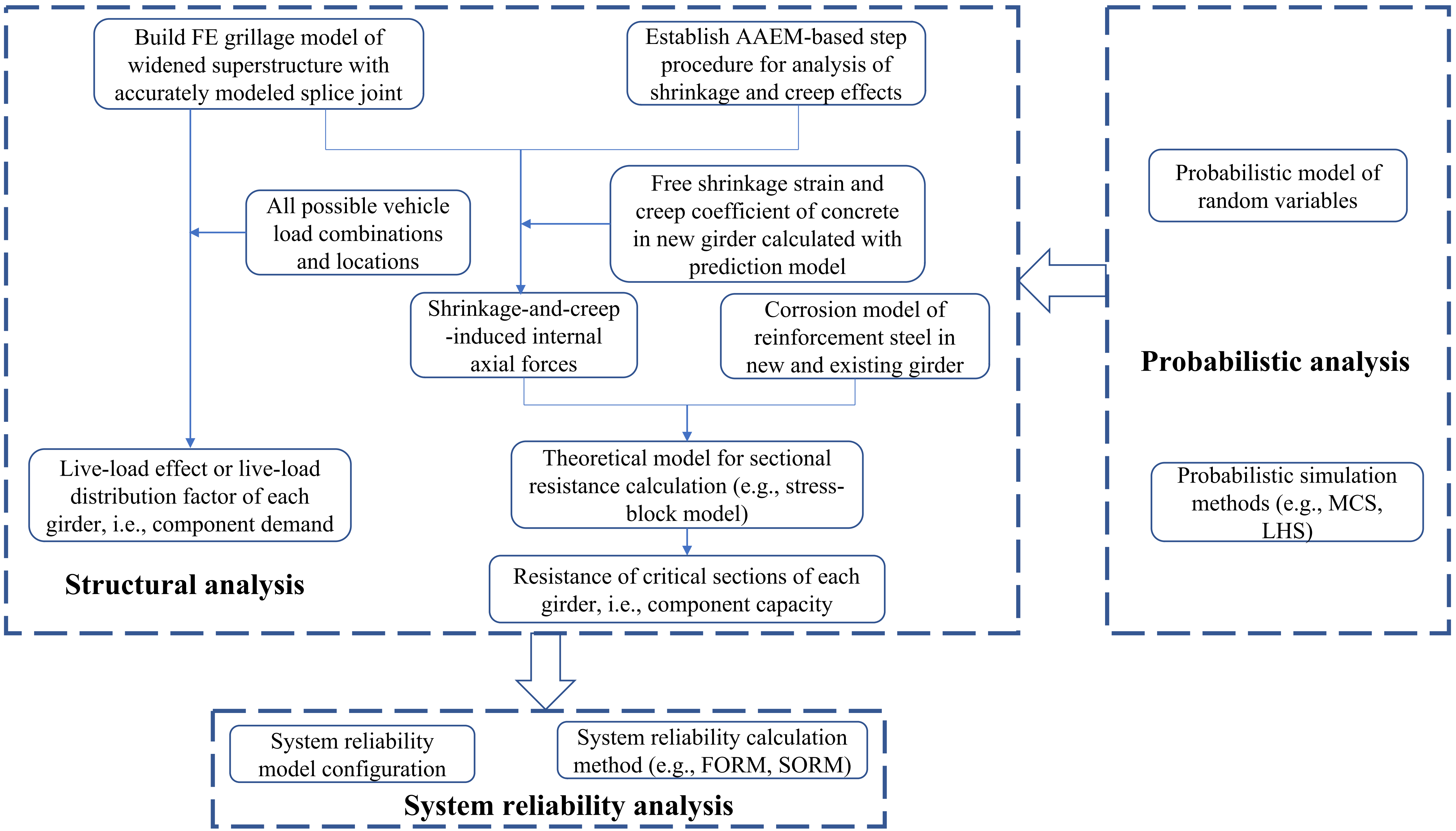
Build FE grillage model of widened superstructure with accurately modeled splice joint
Establish AAEM-based step procedure for analysis of shrinkage and creep effects
Free shrinkage strain and creep coefficient of concrete in new girder calculated with prediction model
All possible vehicle load combinations and locations
Shrinkage-and-creep -induced internal axial forces
Corrosion model of reinforcement steel in new and existing girder
Live-load effect or live-load distribution factor of each girder, i.e., component demand
Theoretical model for sectional resistance calculation (e.g., stress-block model)
Resistance of critical sections of each girder, i.e., component capacity
Structural analysis
Probabilistic model of random variables
Probabilistic analysis
Probabilistic simulation methods (e.g., MCS, LHS)
System reliability model configuration
System reliability calculation method (e.g., FORM, SORM)
System reliability analysis

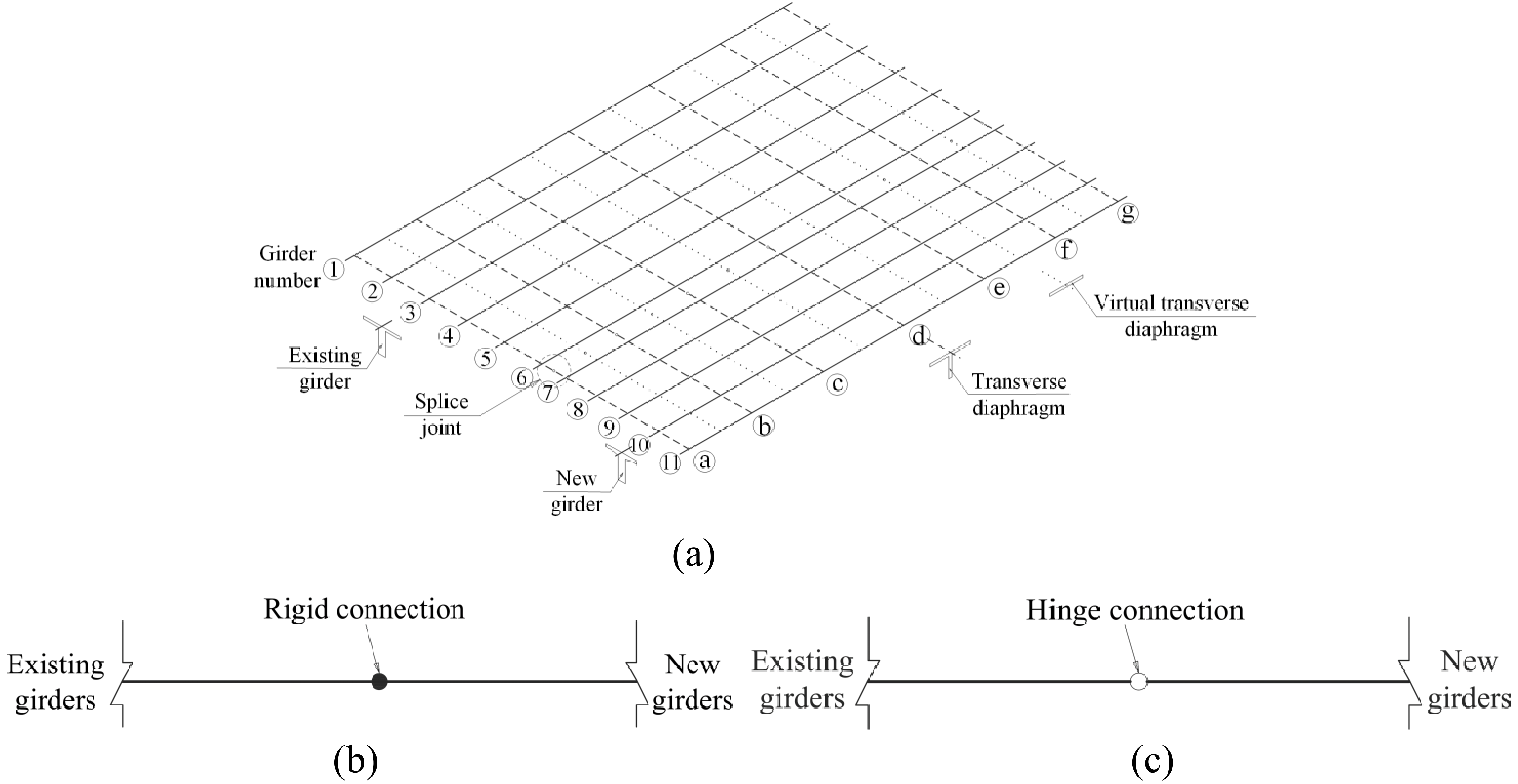
Girder number
1
2
3
4
5
6
7
8
9
10
11
a
b
c
d
e
f
g
Existing girder
Splice joint
New girder
Transverse diaphragm
Virtual transverse diaphragm
(a)
Rigid connection
Existing girders
New girders
(b)
Hinge connection
Existing girders
New girders
(c)

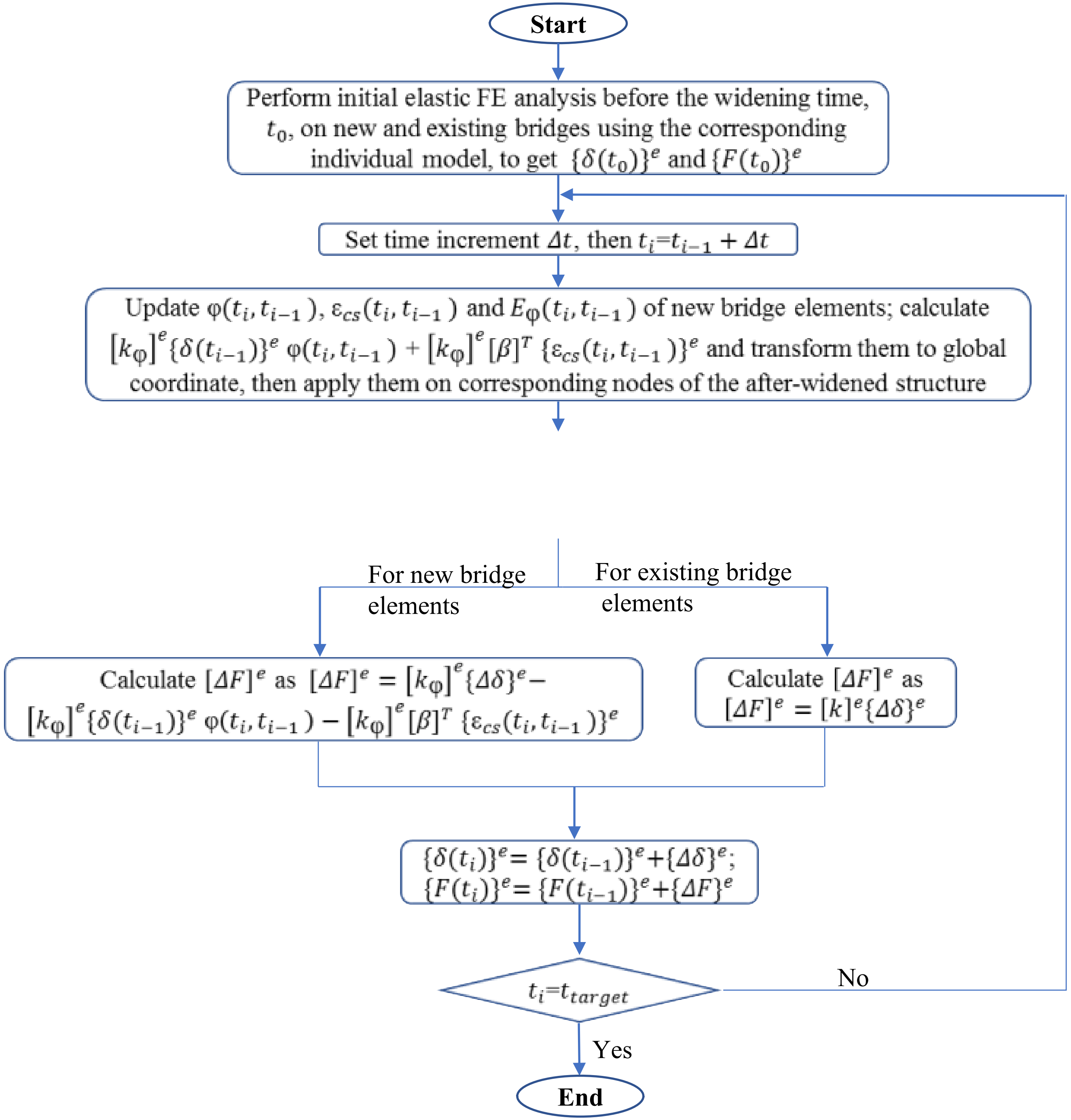
Start
Perform initial elastic FE analysis before the widening time, t_0, on new and existing bridges using the corresponding individual model, to get $\{\delta(t_0)\}^e$ and $\{F(t_0)\}^e$
Set time increment Δt, then t_i=$t_{i-1} + \Delta t$
Update $\varphi(t_i, t_{i-1})$, $\varepsilon_{cs}(t_i, t_{i-1})$ and $E_\varphi(t_i, t_{i-1})$ of new bridge elements; calculate $[k_\varphi]^e\{\delta(t_{i-1})\}^e\ \varphi(t_i, t_{i-1}) + [k_\varphi]^e[\beta]^T\ \{\varepsilon_{cs}(t_i, t_{i-1})\}^e$ and transform them to global coordinate, then apply them on corresponding nodes of the after-widened structure
For new bridge elements
For existing bridge elements
Calculate $[\Delta F]^e$ as $[\Delta F]^e = [k_\varphi]^e\{\Delta\delta\}^e - [k_\varphi]^e\{\delta(t_{i-1})\}^e\ \varphi(t_i, t_{i-1}) - [k_\varphi]^e[\beta]^T\ \{\varepsilon_{cs}(t_i, t_{i-1})\}^e$
Calculate $[\Delta F]^e$ as $[\Delta F]^e = [k]^e\{\Delta\delta\}^e$
$\{\delta(t_i)\}^e = \{\delta(t_{i-1})\}^e + \{\Delta\delta\}^e$;
$\{F(t_i)\}^e = \{F(t_{i-1})\}^e + \{\Delta F\}^e$
t_i=t_{target}
No
Yes
End

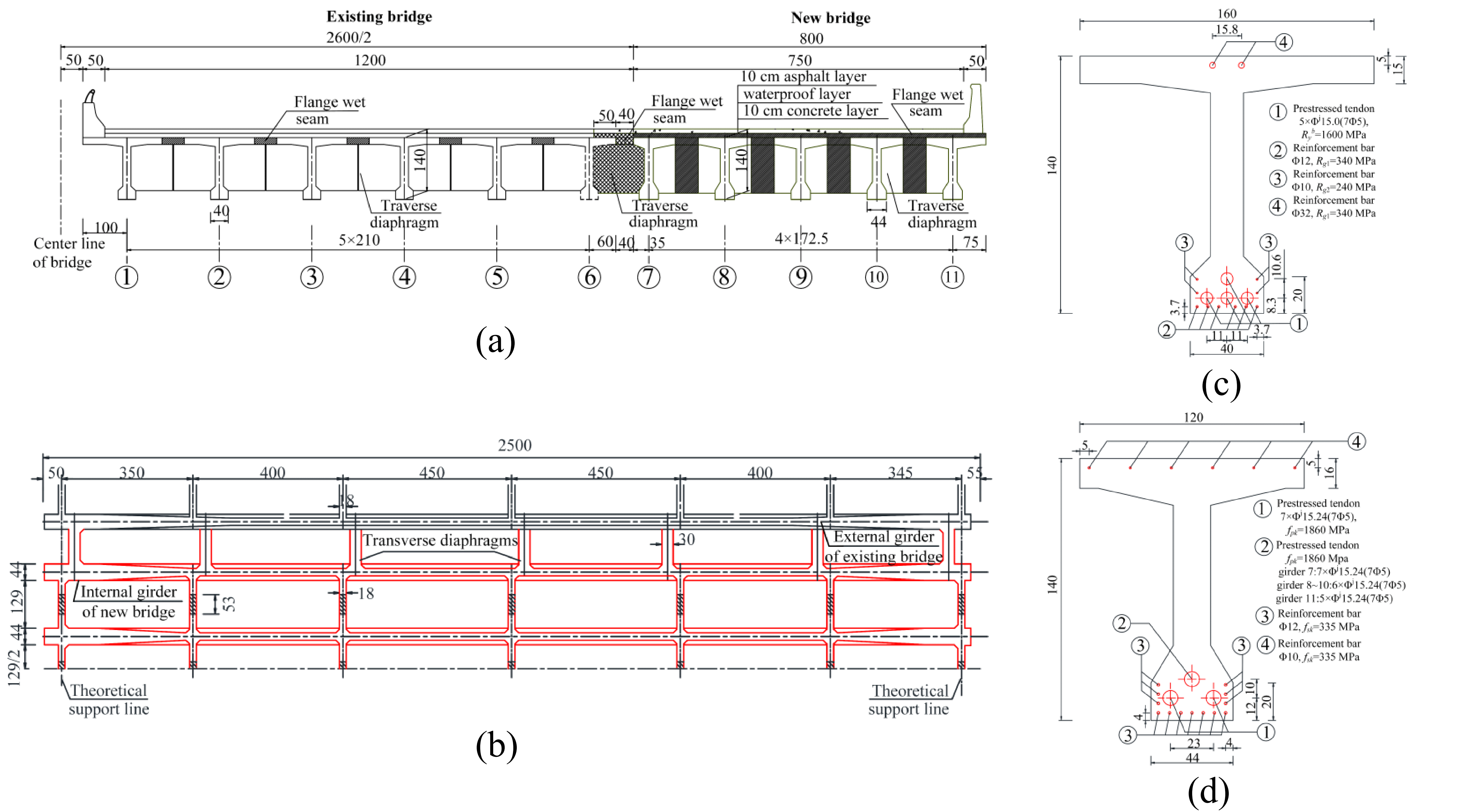
Existing bridge
2600/2
New bridge
800
50 50
1200
750
50
10 cm asphalt layer
waterproof layer
10 cm concrete layer
Flange wet seam
Flange wet seam
Flange wet seam
50 40
140
140
Traverse diaphragm
Traverse diaphragm
Traverse diaphragm
40
44
100
Center line of bridge
5×210
60 40 35
4×172.5
75
① ② ③ ④ ⑤ ⑥ ⑦ ⑧ ⑨ ⑩ ⑪
(a)
2500
50 350 400 450 450 400 345 55
18
Transverse diaphragms
30
External girder of existing bridge
Internal girder of new bridge
53
18
44
129
44
129/2
Theoretical support line
Theoretical support line
(b)
160
15.8
④
5
15
140
① Prestressed tendon 5×Φʲ15.0(7Φ5), R_y^b=1600 MPa
② Reinforcement bar Φ12, R_{g1}=340 MPa
③ Reinforcement bar Φ10, R_{g2}=240 MPa
④ Reinforcement bar Φ32, R_{g1}=340 MPa
10.6
20
8.3
3.7
3.7
11 11
40
(c)
120
5
5
16
140
① Prestressed tendon 7×Φʲ15.24(7Φ5), f_{pk}=1860 MPa
② Prestressed tendon f_{pk}=1860 Mpa girder 7:7×Φʲ15.24(7Φ5) girder 8~10:6×Φʲ15.24(7Φ5) girder 11:5×Φʲ15.24(7Φ5)
③ Reinforcement bar Φ12, f_{sk}=335 MPa
④ Reinforcement bar Φ10, f_{sk}=335 MPa
12 10
20
4
23
4
44
(d)

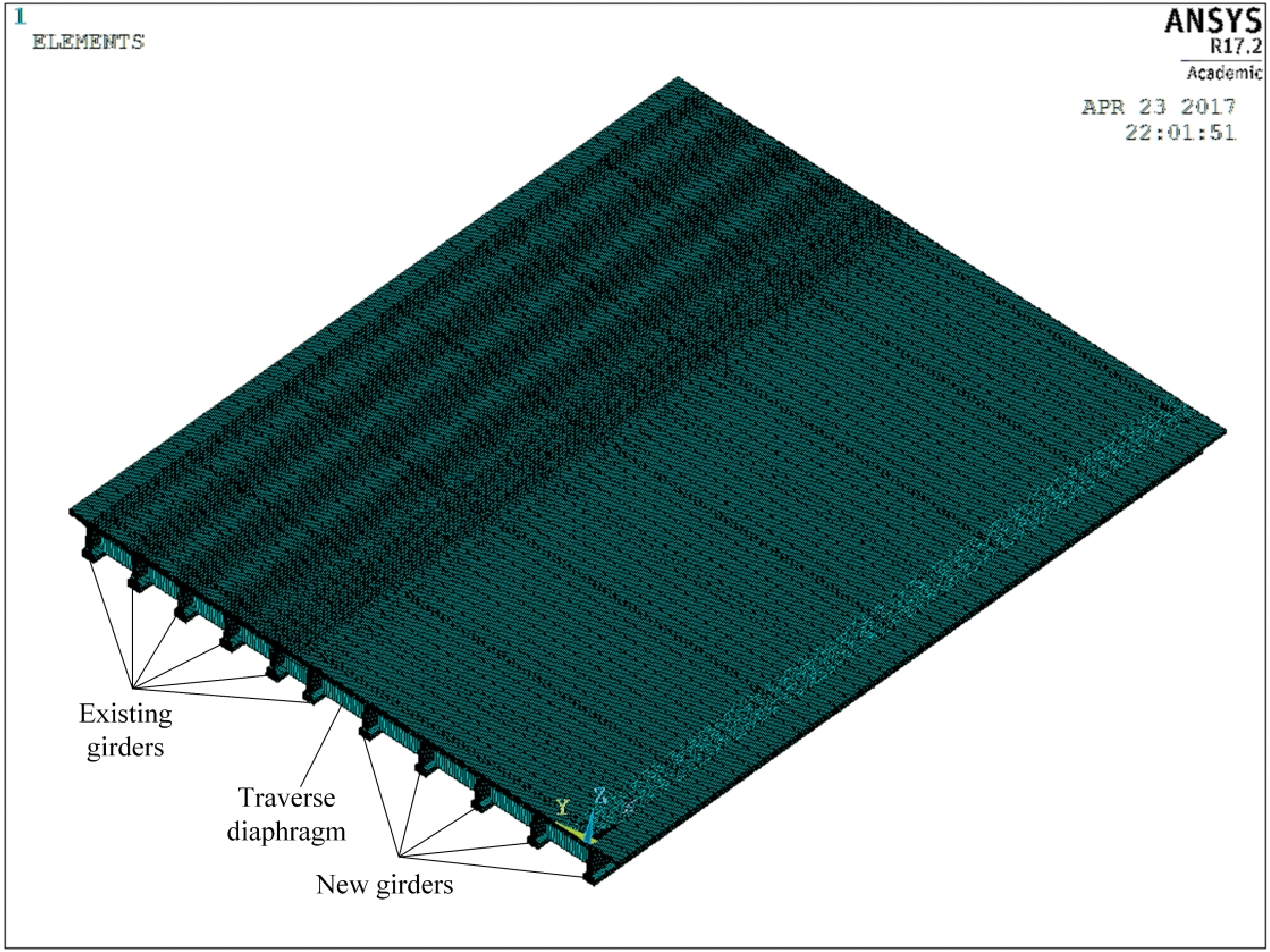
1
ELEMENTS
ANSYS
R17.2
Academic
APR 23 2017
22:01:51
Existing girders
Traverse diaphragm
New girders
Y
Z

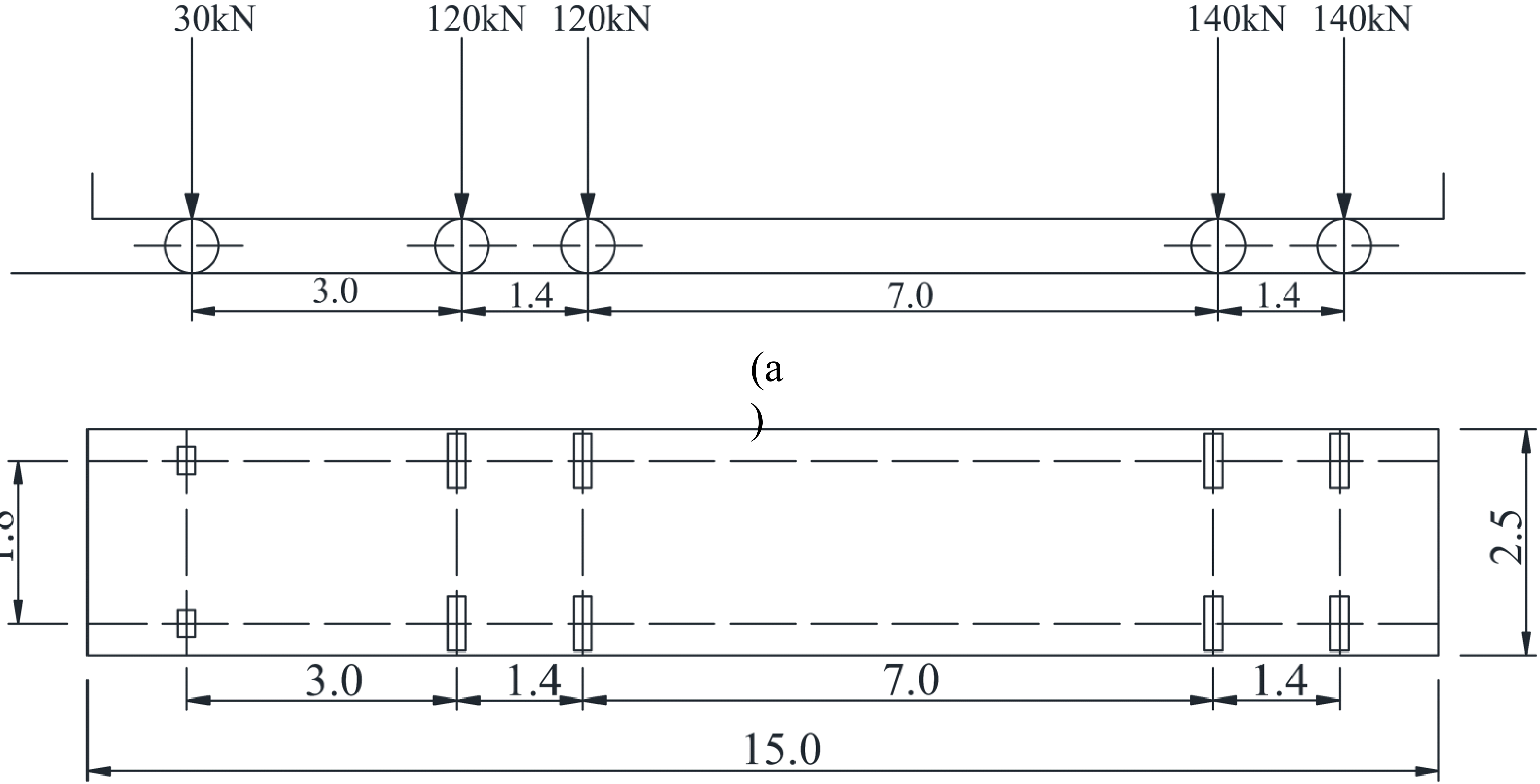

(a)

(b)

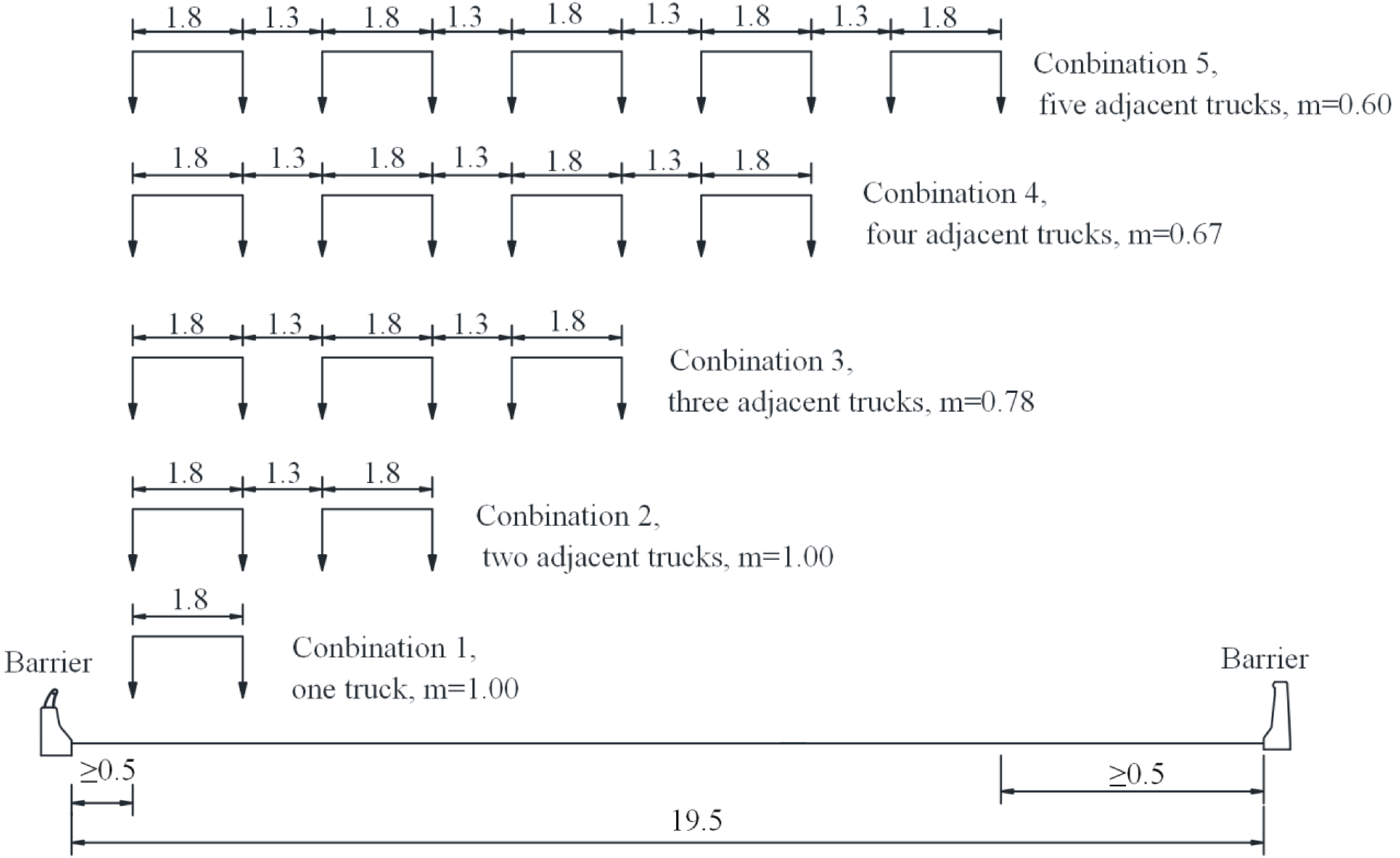
1.8
1.3
1.8
1.3
1.8
1.3
1.8
1.3
1.8
Conbination 5,
five adjacent trucks, m=0.60
Conbination 4,
four adjacent trucks, m=0.67
Conbination 3,
three adjacent trucks, m=0.78
Conbination 2,
two adjacent trucks, m=1.00
Conbination 1,
one truck, m=1.00
Barrier
Barrier
≥0.5
≥0.5
19.5

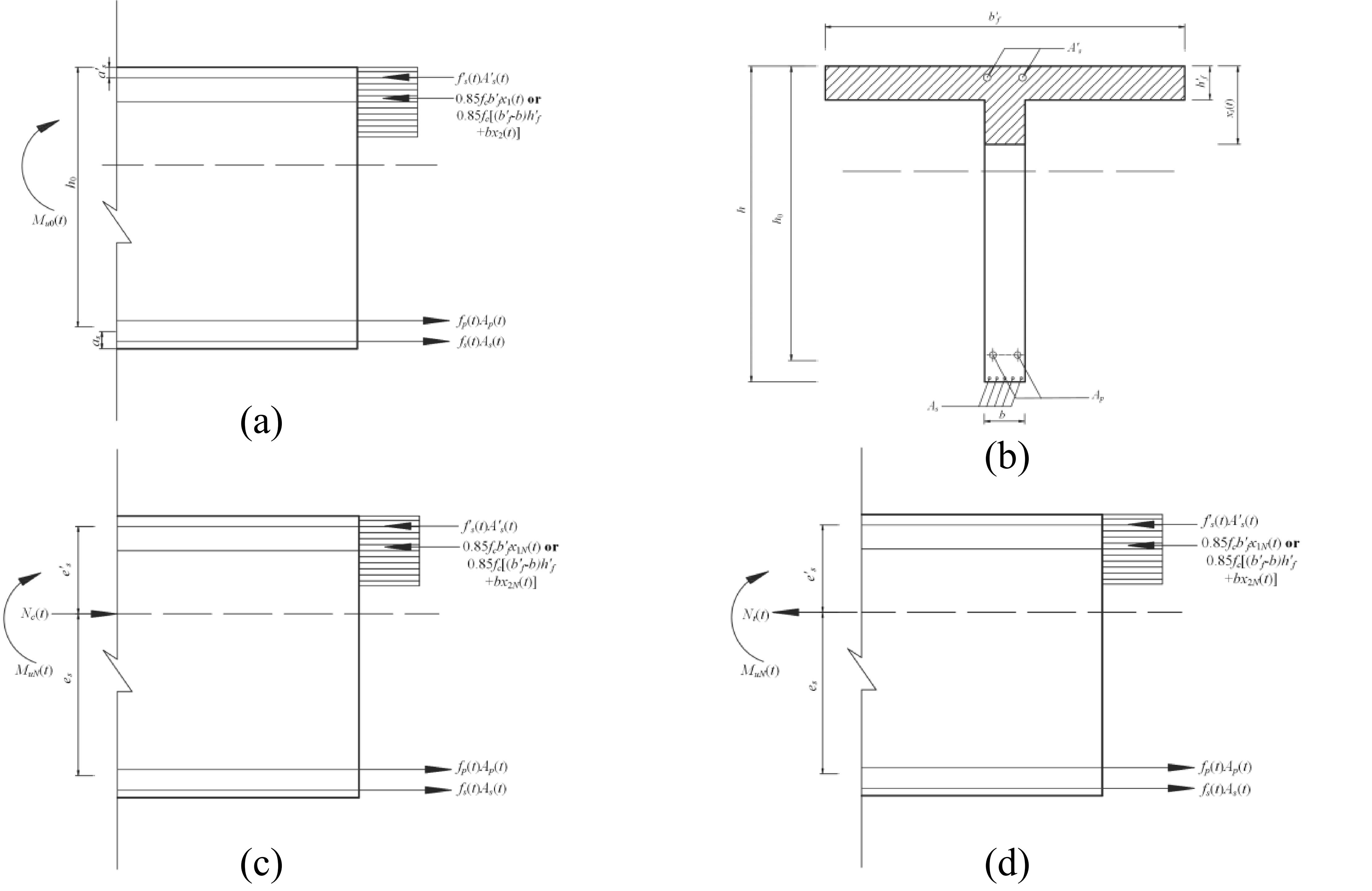

a'_s
$f'_s(t)A'_s(t)$
$0.85f_cb'_fx_1(t)$ or
$0.85f_c[(b'_f-b)h'_f$
$+bx_2(t)]$
h_0
$M_{u0}(t)$
$f_p(t)A_p(t)$
a_s
$f_s(t)A_s(t)$
(a)
b'_f
A'_s
h'_f
$x_1(t)$
h
h_0
A_s
A_p
b
(b)
$f'_s(t)A'_s(t)$
$0.85f_cb'_fx_{1N}(t)$ or
$0.85f_c[(b'_f-b)h'_f$
$+bx_{2N}(t)]$
e'_s
$N_c(t)$
$M_{uN}(t)$
e_s
$f_p(t)A_p(t)$
$f_s(t)A_s(t)$
(c)
$f'_s(t)A'_s(t)$
$0.85f_cb'_fx_{1N}(t)$ or
$0.85f_c[(b'_f-b)h'_f$
$+bx_{2N}(t)]$
e'_s
$N_t(t)$
$M_{uN}(t)$
e_s
$f_p(t)A_p(t)$
$f_s(t)A_s(t)$
(d)

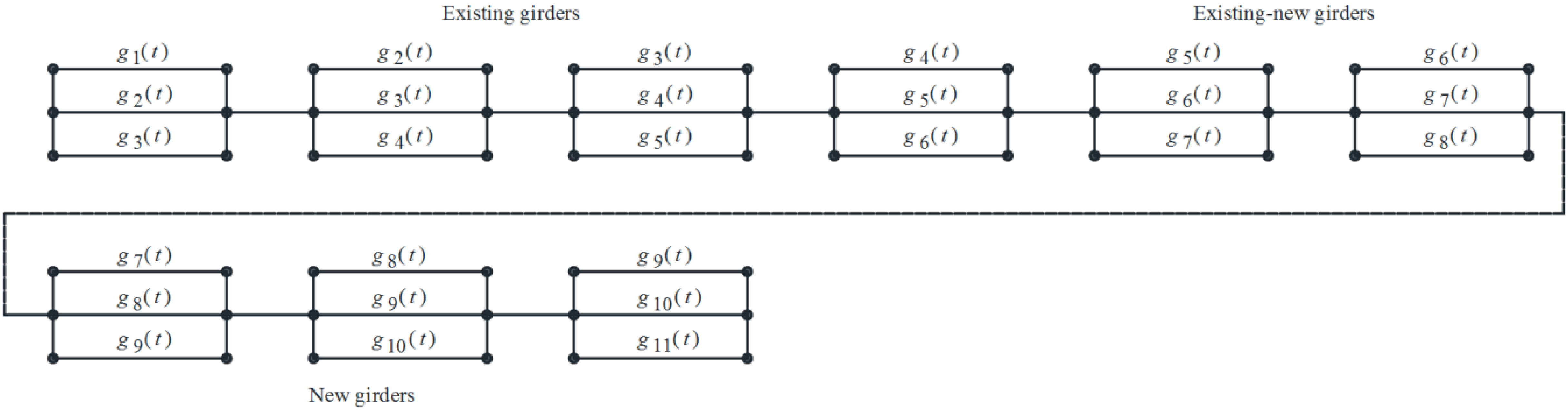
Existing girders
Existing-new girders
$g_1(t)$
$g_2(t)$
$g_3(t)$
$g_4(t)$
$g_5(t)$
$g_6(t)$
$g_7(t)$
$g_8(t)$
$g_9(t)$
$g_{10}(t)$
$g_{11}(t)$
New girders

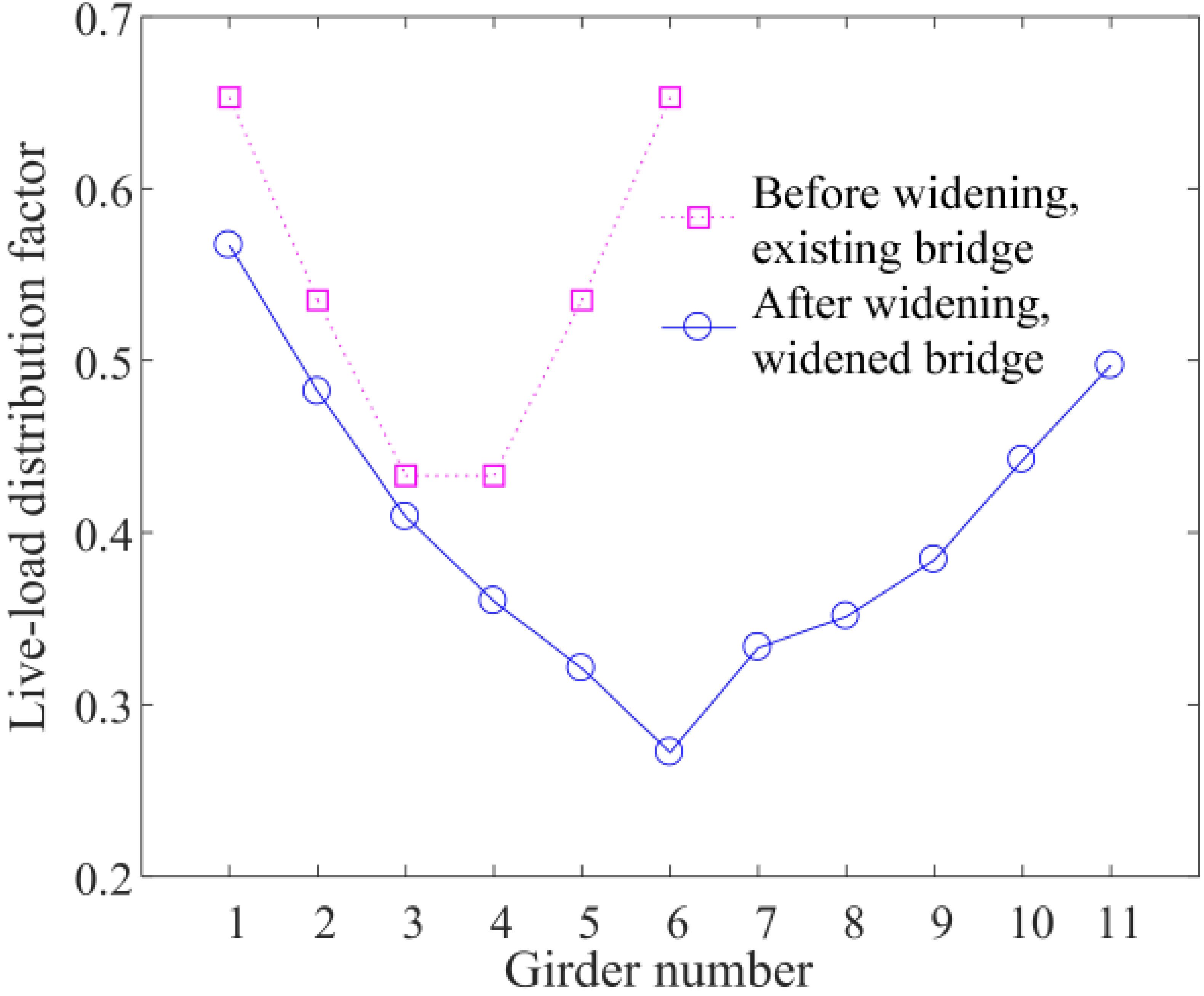

0.7
0.6
0.5
0.4
0.3
0.2
Live-load distribution factor
Before widening, existing bridge
After widening, widened bridge
1
2
3
4
5
6
7
8
9
10
11
Girder number

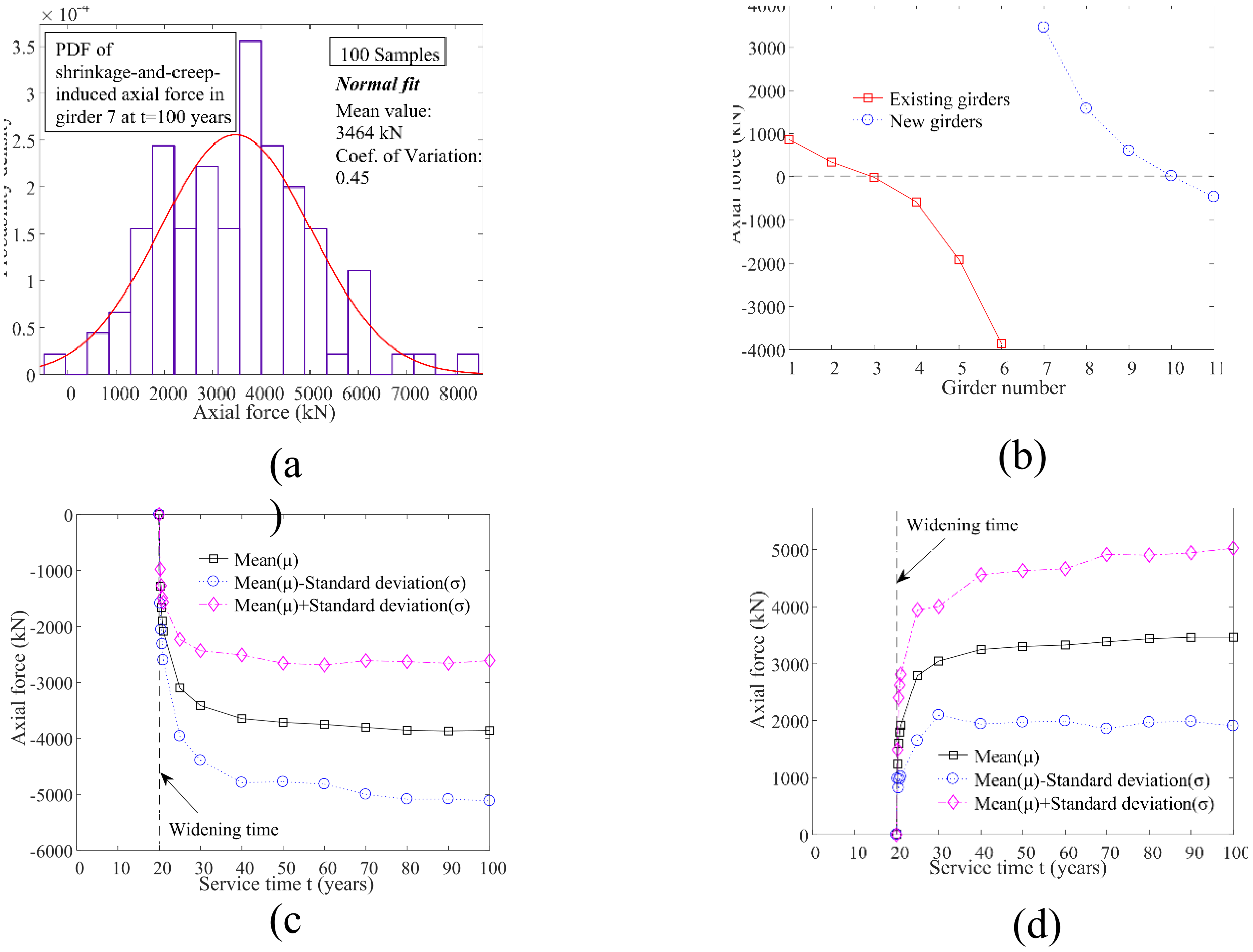

× 10^-4
PDF of shrinkage-and-creep-induced axial force in girder 7 at t=100 years
100 Samples
Normal fit
Mean value: 3464 kN
Coef. of Variation: 0.45
Axial force (kN)
(a)
Existing girders
New girders
Girder number
(b)
Mean(μ)
Mean(μ)-Standard deviation(σ)
Mean(μ)+Standard deviation(σ)
Widening time
Axial force (kN)
Service time t (years)
(c)
Widening time
Mean(μ)
Mean(μ)-Standard deviation(σ)
Mean(μ)+Standard deviation(σ)
Axial force (kN)
Service time t (years)
(d)

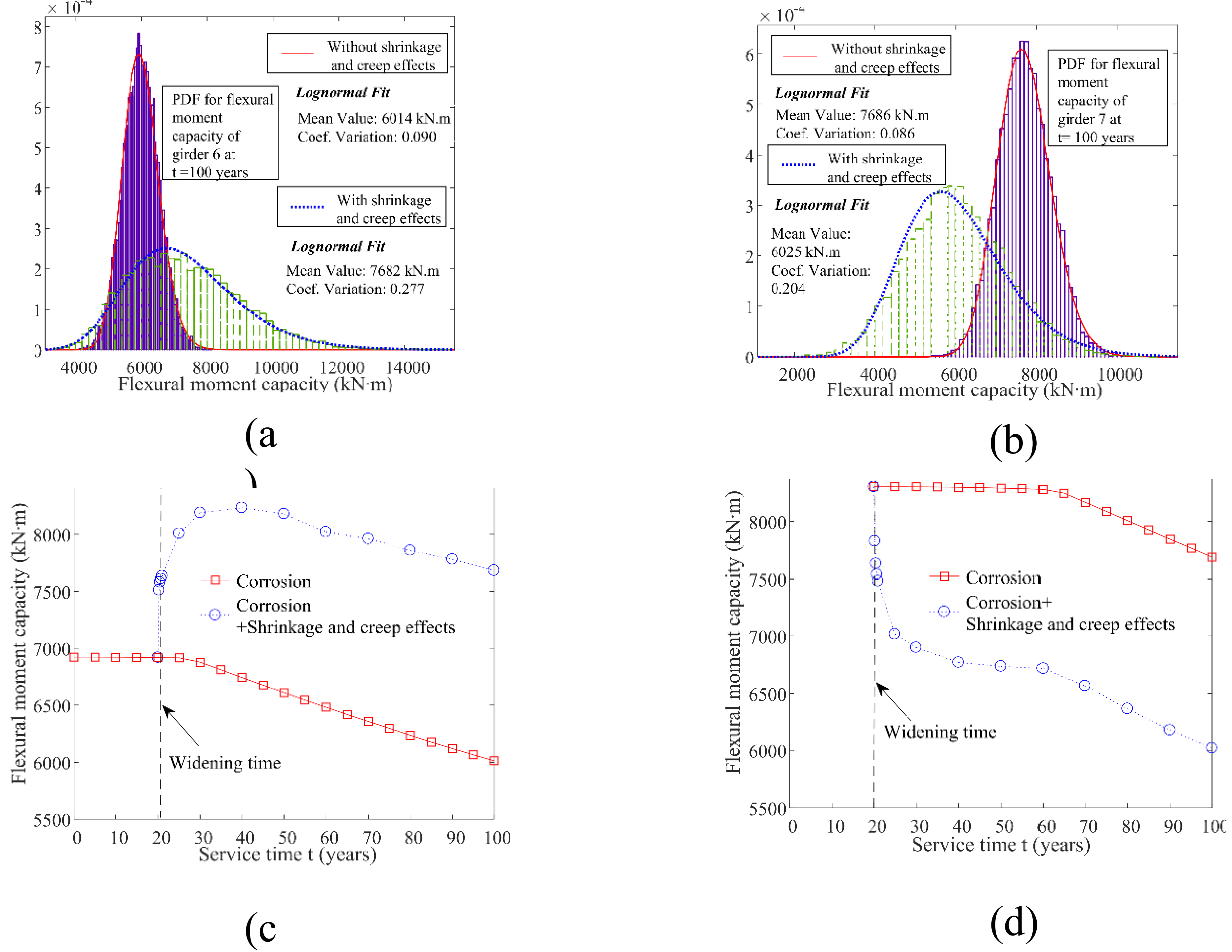

× 10⁻⁴
Without shrinkage and creep effects
PDF for flexural moment capacity of girder 6 at t =100 years
Lognormal Fit
Mean Value: 6014 kN.m
Coef. Variation: 0.090
With shrinkage and creep effects
Lognormal Fit
Mean Value: 7682 kN.m
Coef. Variation: 0.277
Flexural moment capacity (kN·m)
(a)
× 10⁻⁴
Without shrinkage and creep effects
Lognormal Fit
Mean Value: 7686 kN.m
Coef. Variation: 0.086
PDF for flexural moment capacity of girder 7 at t= 100 years
With shrinkage and creep effects
Lognormal Fit
Mean Value: 6025 kN.m
Coef. Variation: 0.204
Flexural moment capacity (kN·m)
(b)
Flexural moment capacity (kN·m)
Corrosion
Corrosion +Shrinkage and creep effects
Widening time
Service time t (years)
(c)
Flexural moment capacity (kN·m)
Corrosion
Corrosion+ Shrinkage and creep effects
Widening time
Service time t (years)
(d)

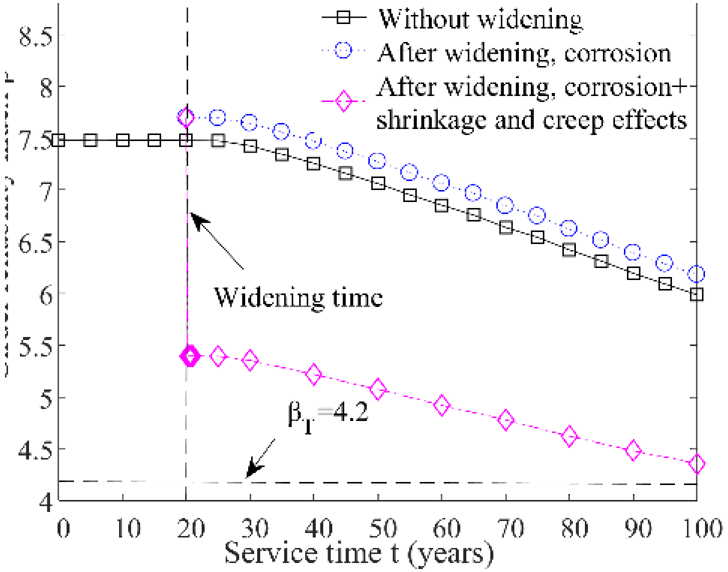
Without widening
After widening, corrosion
After widening, corrosion+ shrinkage and creep effects
Widening time
β_T=4.2
Service time t (years)

(a)

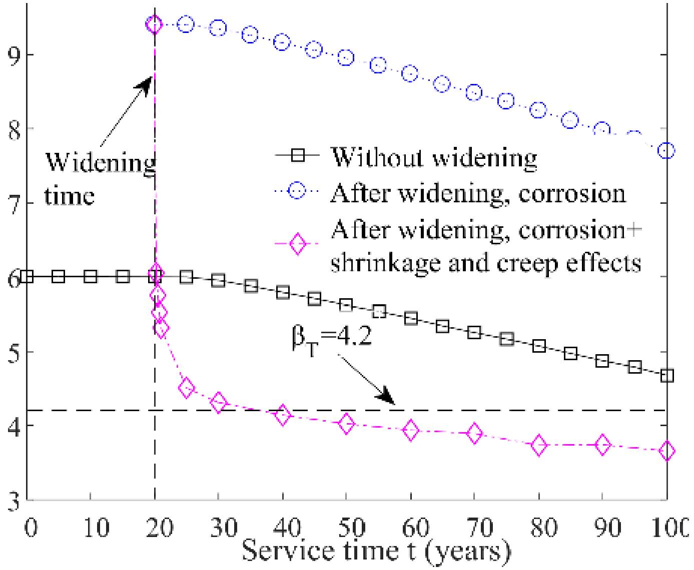
Widening time
Without widening
After widening, corrosion
After widening, corrosion+ shrinkage and creep effects
β_T=4.2
Service time t (years)

(b)

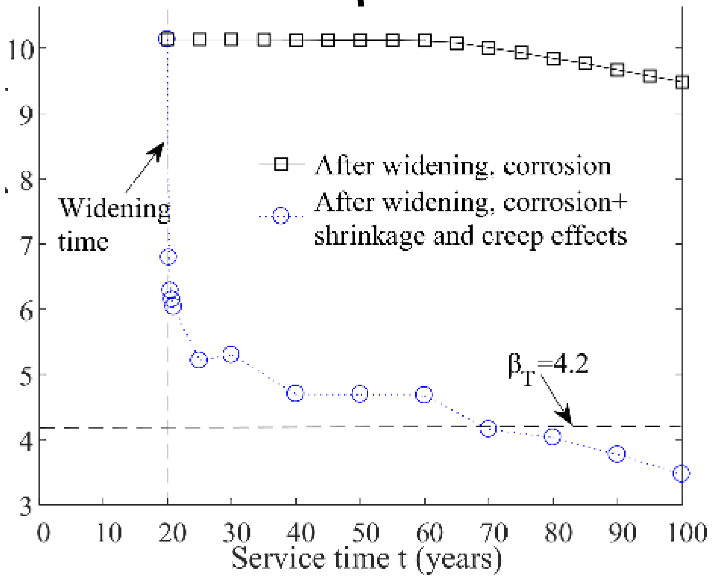
Widening time
After widening, corrosion
After widening, corrosion+ shrinkage and creep effects
β_T=4.2
Service time t (years)

(c)

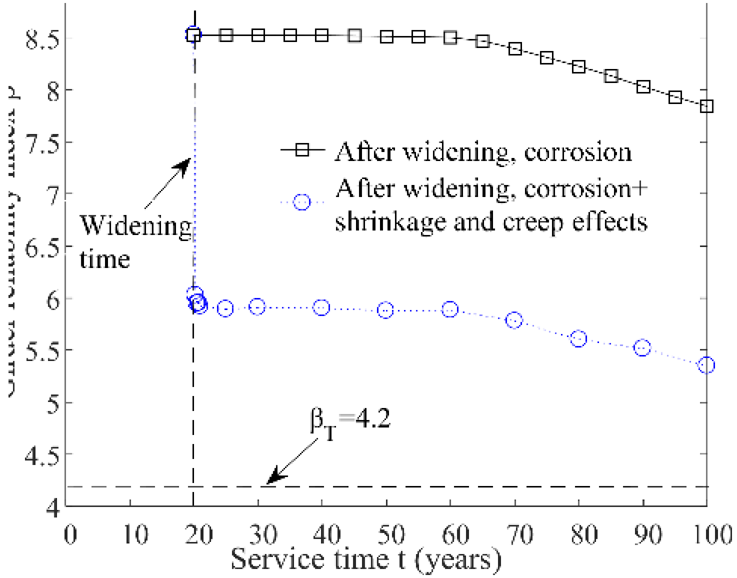
Widening time
After widening, corrosion
After widening, corrosion+ shrinkage and creep effects
β_T=4.2
Service time t (years)

(d)

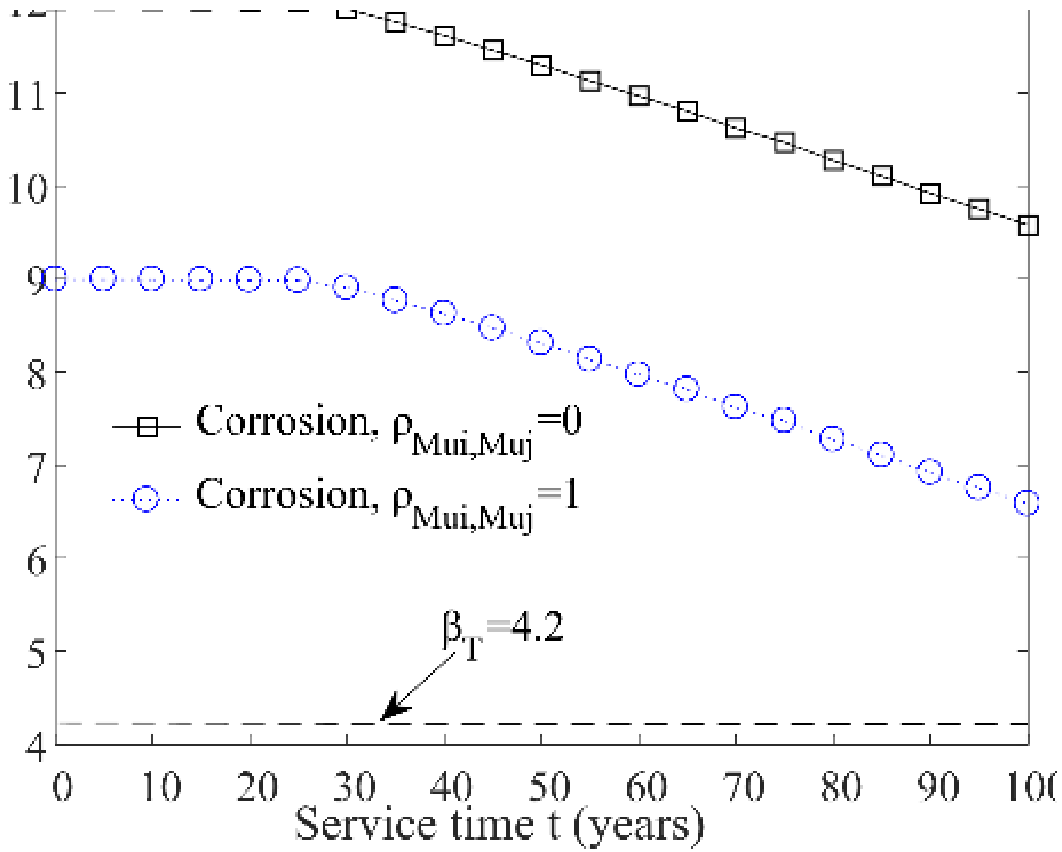

11
10
9
8
7
6
5
4
Corrosion, ρMui,Muj=0
Corrosion, ρMui,Muj=1
βT=4.2
0
10
20
30
40
50
60
70
80
90
100
Service time t (years)

(a
)

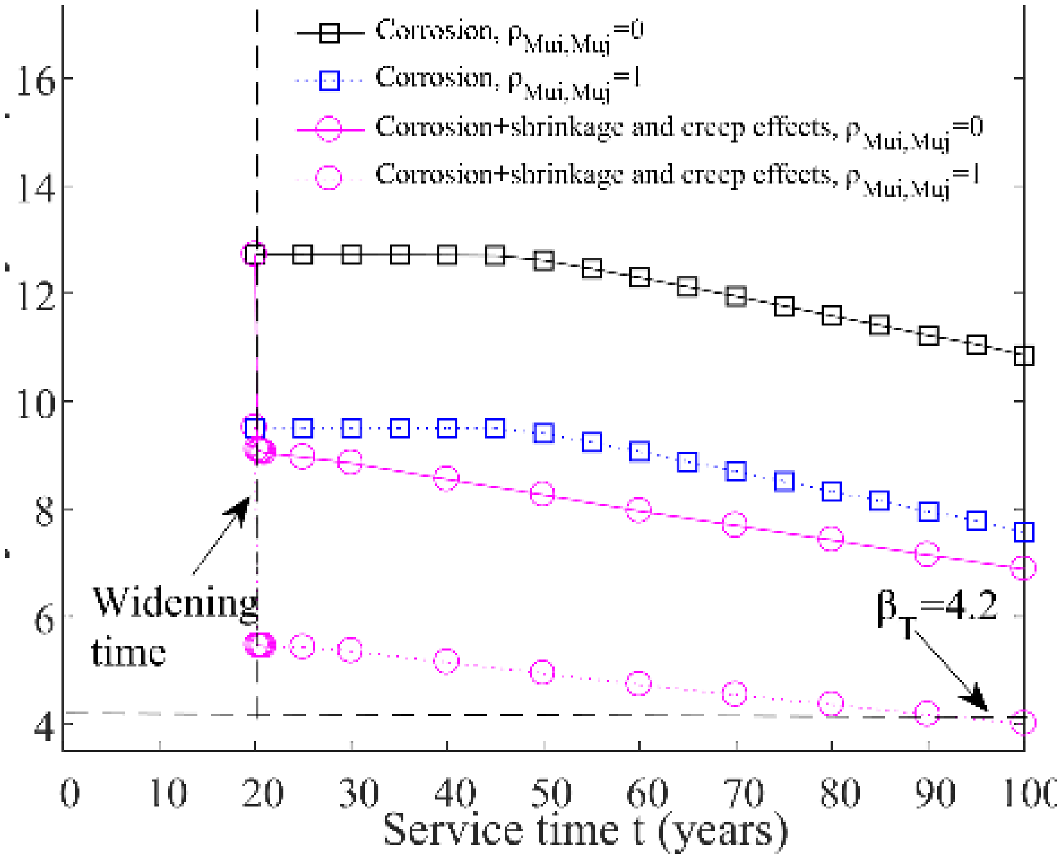

16
14
12
10
8
6
4
Corrosion, ρMui,Muj=0
Corrosion, ρMui,Muj=1
Corrosion+shrinkage and creep effects, ρMui,Muj=0
Corrosion+shrinkage and creep effects, ρMui,Muj=1
Widening time
βT=4.2
0
10
20
30
40
50
60
70
80
90
100
Service time t (years)

(b)